A higher-order finite-element implementation of the full-F Landau Fokker-Planck collision operator for charged particle collisions in a low density plasma

M. R. Hardman[1,2]**, M. Abazorius**[2]**, J. Omotani**[3]**, M. Barnes**[2]**, S. L. Newton**[3]**, and F. I. Parra**[4]

[1] Tokamak Energy Ltd, 173 Brook Drive, Milton Park, Abingdon, OX14 4SD, United Kingdom
[2] Rudolf Peierls Centre for Theoretical Physics, University of Oxford, Clarendon Laboratory, Parks Road, Oxford OX1 3PU, United Kingdom
[3] United Kingdom Atomic Energy Authority, Culham Science Centre, Abingdon, Oxon, OX14 3DB, UK
[4] Princeton Plasma Physics Laboratory, P.O. Box 451, Princeton, New Jersey 08540, United States

E-mail: `michael.hardman@tokamakenergy.co.uk`

1. Introduction

A low density plasma is one that can be accurately described by the one-point particle probability distribution function $F_s(\mathbf{r}, \mathbf{v})$. The distribution function provides us with the probability $p = F_s(\mathbf{r}, \mathbf{v}) \; d^3\mathbf{r} d^3\mathbf{v}$ to find a particle of species s in the phase space volume around the phase space position $(\mathbf{r}, \mathbf{v})$, with $\mathbf{r}$ the particle position and $\mathbf{v}$ the particle velocity. An equation for the distribution function may be obtained from the BBGKY hierarchy [1, 2], which converts an N-body Hamiltonian system describing a plasma or gas into a statistical description. The resulting equation has the form

$$\frac{\partial F_s}{\partial t} + \mathbf{v} \cdot \nabla F_s + \frac{Z_s e}{m_s} \left(\mathbf{E} + \mathbf{v} \times \mathbf{B}\right) \cdot \frac{\partial F_s}{\partial \mathbf{v}} = \sum_{s'} C_{ss'} \left[F_s, F_{s'}\right], \tag{1}$$

where the left-hand side of the equation is the Vlasov equation, accounting for the acceleration of particles by the large-scale electromagnetic fields, and the Boltzmann collision operator on the right-hand side of the equation accounts for the interactions of particles of species s with local small-scale electromagnetic fields generated by interactions between particles of differing species s' at the same position $\mathbf{r}$. Here, m_s is the species mass, Z_s is the species charge number, e is the unit charge, and $\mathbf{E}$ and $\mathbf{B}$ are the electric and magnetic fields, respectively,

If the interaction cross section is chosen to be the $1/r^2$ electrostatic potential, then the collision operator becomes the well-known Landau Fokker-Planck collision operator

[3, 4, 5, 6]:

$$C_{ss'}\left[F_s, F_{s'}\right] = \frac{\gamma_{ss'}}{m_s} \frac{\partial}{\partial \mathbf{v}} \cdot \left\{ \int \frac{\partial^2 g}{\partial \mathbf{v} \partial \mathbf{v}} \cdot \left[\frac{F_{s'}(\mathbf{v}')}{m_s} \frac{\partial F_s}{\partial \mathbf{v}} - \frac{F_s(\mathbf{v})}{m_{s'}} \frac{\partial F_{s'}}{\partial \mathbf{v}'} \right] d^3 \mathbf{v}' \right\}, \tag{2}$$

where

$$\gamma_{ss'} = \frac{2\pi Z_s^2 Z_{s'}^2 e^4 \ln \Lambda_{ss'}}{(4\pi\epsilon_0)^2}, \tag{3}$$

with $\ln \Lambda_{ss'}$ the Coulomb logarithm [3, 6, 4, 5], and

$$g = |\mathbf{v} - \mathbf{v}'|. \tag{4}$$

The operator is integro-differential because the effect of small-angle collisions dominate over the rarer large-angle collisions. The complex structure of the collision operator obscures four key properties that we note. First, the collision operator conserves particle density, i.e.,

$$\int C_{ss'}\left[F_s, F_{s'}\right] d^3 \mathbf{v} = 0. \tag{5}$$

Second, the collision operator conserves the total momentum in a collision, i.e.,

$$\int \left(m_s \mathbf{v} \, C_{ss'}\left[F_s, F_{s'}\right] + m_{s'} \mathbf{v} \, C_{s's}\left[F_{s'}, F_s\right] \right) d^3 \mathbf{v} = 0. \tag{6}$$

The same is true for the total energy:

$$\int \left(\frac{1}{2} m_s |\mathbf{v}|^2 \, C_{ss'}\left[F_s, F_{s'}\right] + \frac{1}{2} m_{s'} |\mathbf{v}|^2 \, C_{s's}\left[F_{s'}, F_s\right] \right) d^3 \mathbf{v} = 0. \tag{7}$$

Finally, Boltzmann's H-theorem applied to same-species collisions [5, 6, 2] proves that the entropy production

$$\dot{S}_s = - \int \ln F_s \, C_{ss}\left[F_s, F_s\right] \, d^3 \mathbf{v} \geq 0 \tag{8}$$

with equality if and only if F_s is a Maxwellian distribution described by the local density n_s, mean velocity $\mathbf{u}_s$, and temperature T_s, i.e.,

$$F_s = F_s^M = \frac{n_s}{\pi^{3/2} v_{\text{th},s}^2} \exp\left[-\left(\frac{\mathbf{v} - \mathbf{u}_s}{v_{\text{th},s}} \right)^2 \right], \tag{9}$$

with $v_{\text{th},s} = \sqrt{2T_s/m_s}$.

Implementing the full Landau collision operator is challenging because of the nonlinear and integro-differential nature of the operator. For a given distribution function F_s, we must carry out a series of difficult integrals to find the coefficients of the operator. Whilst previous authors have implemented the full operator, see, e.g., [7, 8, 9, 10], including implementations of the underlying Boltzmann operator [11], it is more typical to use asymptotic expansions to linearised the operator for its use in a

specific application (e.g. transport theory or collisional closures [4, 5, 12, 13]). It is also common to write down an ad-hoc diffusive model operator which may be solved rapidly yet still has the conservation or H-theorem properties desired for the physics of interest [14, 15, 16, 17].

In core-transport plasma turbulence applications, collisional relaxation timescales are typically long compared to the non-linear turnover time of the turbulent eddies, meaning that the linearised Landau operator or ad-hoc model operators are an appropriate cost saving device: physically, all these operators are required to do is dissipate fine velocity-space structure [15, 16]. The system is known to be approximately in thermal equilibrium because the system is closed [13, 18], meaning that the distribution function is never far from the Maxwellian around which the collision operator is easily linearised. However, in the scrape-off layer the distribution function of the bulk plasma may well be far from Maxwellian. This is due to the presence of the divertor plate or limiter, which makes the system open, preventing local thermal equilibrium. In addition, hot particles may transit rapidly from the core to the open field lines at the edge where the bulk of the plasma is expected to be cooler, potentially resulting in a bimodal distribution of particle energies. In general, the exact steady state distribution is not known. In summary, it is not clear whether or not a model or linearised collision operator is adequate for modelling the plasma on open field lines. The only rigorous choice of operator is the full-F Landau operator.

In this report we describe the implementation of the full-F Landau operator using higher-order finite elements for gyrotropic distribution functions. Gyrotropic distributions are independent of the gyrophase angle ϑ that measures the position of the particle in the plane perpendicular to the magnetic field. Mathematically, this means that we support $F_s = F_s(v_\parallel, v_\perp)$, with the cylindrical velocity space coordinates $(v_\parallel, v_\perp, \vartheta)$ defined by

$$v_\parallel = \mathbf{v} \cdot \mathbf{b}, \quad v_\perp = |\mathbf{v} - v_\parallel \mathbf{b}|, \quad \tan \vartheta = -\frac{\mathbf{v} \cdot \mathbf{e}_2}{\mathbf{v} \cdot \mathbf{e}_1}, \tag{10}$$

or equivalently,

$$\mathbf{v} = v_\parallel \mathbf{b} + v_\perp (\cos \vartheta \mathbf{e}_1 - \sin \vartheta \mathbf{e}_2). \tag{11}$$

The basis vector $\mathbf{b} = \mathbf{B}/|\mathbf{B}|$ is the unit vector in the direction of the magnetic field. The vectors $\mathbf{e}_1$ and $\mathbf{e}_2$ are orthogonal to $\mathbf{b}$ and satisfy

$$\mathbf{b} \cdot \mathbf{e}_1 \times \mathbf{e}_2 = 1, \quad \mathbf{e}_1 \cdot \mathbf{b} = 0, \quad \mathbf{e}_2 \cdot \mathbf{b} = 0. \tag{12}$$

The numerical implementation described in this report ensures the satisfaction of the conservative properties (5)-(7) by achieving high accuracy with the weak formulations and adequate numerical resolution. Almost exact numerical conservation is obtained with ah-hoc numerical conserving terms, which are necessary to preserve a stable solution at long times. To avoid carrying out costly numerical integration to find the coefficients in the whole of the velocity space, we use the Rosenbluth-MacDonald-Judd (RMJ) form of the collision operator (which is a Fokker-Planck form) [3] and we

solve elliptic PDEs for the required coefficients, called Rosenbluth potentials, using the higher-order finite element method and boundary conditions obtained from the Green's functions at the limits of the velocity space. This numerical strategy optimises the scheme for scalability.

The remainder of the report is structured as follows. In the next section, we write the collision operator in the RMJ form. In section 3, we obtain the weak-form representation of the problem that we will implement numerically. In section 4 we discuss the boundary conditions imposed on F_s during an explicit time advance. In section 5 we prescribe numerical conserving terms for use in the time advance. In section 6 we provide numerical results from testing our implementation. In section 7, we discuss the outlook for the use of the operator in a production code. Finally, Appendix A and Appendix B contain useful results pertaining to numerical integration of the Green's functions of the derivatives of the Rosenbluth potentials.

2. Rosenbluth-MacDonald-Judd form of the collision operator

The operator in the Rosenbluth-MacDonald-Judd (RMJ) form [3, 6] in $(v_\parallel, v_\perp)$ coordinates is most usefully written in terms of collisional fluxes:

$$C_{ss'}\left[F_s, F_{s'}\right] = \frac{\partial \Gamma_\parallel}{\partial v_\parallel} + \frac{1}{v_\perp} \frac{\partial}{\partial v_\perp}\left(v_\perp \Gamma_\perp\right). \tag{13}$$

where the fluxes are defined by

$$\Gamma_\parallel = \frac{\gamma_{ss'}}{m_s^2}\left(\frac{\partial F_s}{\partial v_\parallel}\frac{\partial^2 G_{s'}}{\partial v_\parallel{}^2} + \frac{\partial F_s}{\partial v_\perp}\frac{\partial^2 G_{s'}}{\partial v_\perp \partial v_\parallel} - 2\frac{m_s}{m_{s'}}F_s\frac{\partial H_{s'}}{\partial v_\parallel}\right), \tag{14}$$

and

$$\Gamma_\perp = \frac{\gamma_{ss'}}{m_s^2}\left(\frac{\partial F_s}{\partial v_\parallel}\frac{\partial^2 G_{s'}}{\partial v_\parallel \partial v_\perp} + \frac{\partial F_s}{\partial v_\perp}\frac{\partial^2 G_{s'}}{\partial v_\perp{}^2} - 2\frac{m_s}{m_{s'}}F_s\frac{\partial H_{s'}}{\partial v_\perp}\right), \tag{15}$$

and the Rosenbluth potentials are

$$G_{s'}(\mathbf{v}) = \int F_{s'}(\mathbf{v}')g \, d^3\mathbf{v}' \tag{16}$$

and

$$H_{s'}(\mathbf{v}) = \int \frac{F_{s'}(\mathbf{v}')}{g} \, d^3\mathbf{v}'. \tag{17}$$

In the drift-kinetic limit the largest piece of the distribution functions are independent of gyroangle [4, 19], i.e., $F_s = F_s(v_\parallel, v_\perp)$ and $F_{s'} = F_{s'}(v_\parallel, v_\perp)$. In terms of $(v_\parallel, v_\perp)$ coordinates, for gyrotropic distributions the Rosebluth potentials simplify to

$$G_{s'} = \int_0^\infty \int_{-\infty}^\infty 4\left(\left(v_\parallel - v_\parallel'\right)^2 + \left(v_\perp + v_\perp'\right)^2\right)^{1/2} E(m(v_\parallel, v_\perp, v_\parallel', v_\perp'))F_{s'}(v_\parallel', v_\perp')v_\perp' \, dv_\parallel' dv_\perp', \tag{18}$$

and

$$H_{s'} = \int_0^\infty \int_{-\infty}^\infty 4 \left(\left(v_\parallel - v'_\parallel \right)^2 + \left(v_\perp + v'_\perp \right)^2 \right)^{-1/2} K(m(v_\parallel, v_\perp, v'_\parallel, v'_\perp)) F_{s'}(v'_\parallel, v'_\perp) v'_\perp \, dv'_\parallel dv'_\perp, \tag{19}$$

where

$$m(v_\parallel, v_\perp, v'_\parallel, v'_\perp) = 4 v_\perp v'_\perp \left(\left(v_\parallel - v'_\parallel \right)^2 + \left(v_\perp + v'_\perp \right)^2 \right)^{-1}, \tag{20}$$

and we have used the definitions of the complete elliptic integral of the first kind

$$K(m) = \int_0^{\pi/2} \frac{1}{\sqrt{1 - m \sin^2 \theta}} \, d\theta \tag{21}$$

and the complete elliptic integral of the second kind

$$E(m) = \int_0^{\pi/2} \sqrt{1 - m \sin^2 \theta} \, d\theta. \tag{22}$$

2.1. Finding elliptic problems for the Rosenbluth potentials

As noted in the original derivation by Rosenbluth, MacDonald, and Judd, [3], the potentials defined by eqations (16) and (17) may also be defined as the solutions of the elliptic problems

$$\frac{\partial^2 G}{\partial v_\parallel^2} + \frac{1}{v_\perp} \frac{\partial}{\partial v_\perp} \left(v_\perp \frac{\partial G}{\partial v_\perp} \right) = 2H, \tag{23}$$

and

$$\frac{\partial^2 H}{\partial v_\parallel^2} + \frac{1}{v_\perp} \frac{\partial}{\partial v_\perp} \left(v_\perp \frac{\partial H}{\partial v_\perp} \right) = -4\pi F. \tag{24}$$

We recognise the Poisson's equation for the Rosenbluth potential H, and the biharmonic equation for G. Obtaining the Rosenbluth potentials through an elliptic solve is potentially numerically advantageous compared to evaluating the Green's function directly. This is because sparse matrix methods can be used to invert the Laplacian operator, giving an operation scaling of N^2, where N is the size of one of the velocity dimensions, whereas a direct evaluation of the Green's function leads to a scaling of the order of N^4. An important detail is that for a finite simulation domain, adequate boundary conditions must be supplied when carrying out the elliptic solve. In practice this necessitates the order N^3 operation of obtaining the boundary data through the Green's function. An order N improvement in the overall scaling is not to be dismissed, and parallelisation over many processes may be able to alleviate a further order N (corresponding to the size of the boundary in velocity space) as evaluating the boundary data is embarrassingly parallel.

Having motivated finding the coefficients appearing in the collision operator through elliptic solves, it remains to find the appropriate PDEs. Direct differentiation of equations (23) and (24) yields the required differential definitions of the coefficients, as we now demonstrate. We can solve for

$$G_{20} = \frac{\partial^2 G}{\partial v_\parallel^2} \tag{25}$$

by simply differentiating equation (23) to find

$$\frac{\partial^2 G_{20}}{\partial v_\parallel{}^2} + \frac{1}{v_\perp} \frac{\partial}{\partial v_\perp} \left(v_\perp \frac{\partial G_{20}}{\partial v_\perp} \right) = 2 \frac{\partial^2 H}{\partial v_\parallel{}^2}. \tag{26}$$

The next coefficient that we require is

$$G_{01} = \frac{\partial G}{\partial v_\perp}. \tag{27}$$

To obtain an elliptic equation for G_{01} we differentiate equation (23) with respect to $v_\perp$ to find that

$$\frac{\partial^2 G_{01}}{\partial v_\parallel{}^2} + \frac{\partial^2 G_{01}}{\partial v_\perp{}^2} + \frac{\partial}{\partial v_\perp} \left(\frac{G_{01}}{v_\perp} \right) = 2 \frac{\partial H}{\partial v_\perp}. \tag{28}$$

Using the identity

$$\frac{\partial^2 G}{\partial v_\perp{}^2} = \frac{1}{v_\perp} \frac{\partial}{\partial v_\perp} \left(v_\perp \frac{\partial G}{\partial v_\perp} \right) - \frac{1}{v_\perp} \frac{\partial G}{\partial v_\perp}, \tag{29}$$

we can rewrite the equation for G_{01} in a form amenable to integration by parts:

$$\frac{\partial^2 G_{01}}{\partial v_\parallel{}^2} + \frac{1}{v_\perp} \frac{\partial}{\partial v_\perp} \left(v_\perp \frac{\partial G_{01}}{\partial v_\perp} \right) - \frac{G_{01}}{v_\perp^2} = 2 \frac{\partial H}{\partial v_\perp}. \tag{30}$$

The next coefficient that we require is

$$G_{11} = \frac{\partial^2 G}{\partial v_\parallel \partial v_\perp}. \tag{31}$$

The differential equation that defines G_{11} may be obtained from (30) by direct differentiation. The result is

$$\frac{\partial^2 G_{11}}{\partial v_\parallel{}^2} + \frac{1}{v_\perp} \frac{\partial}{\partial v_\perp} \left(v_\perp \frac{\partial G_{11}}{\partial v_\perp} \right) - \frac{G_{11}}{v_\perp^2} = 2 \frac{\partial^2 H}{\partial v_\parallel \partial v_\perp}. \tag{32}$$

To complete the set of coefficients derived from G, an algebraic equation for

$$G_{02} = \frac{\partial^2 G}{\partial v_\perp{}^2} \tag{33}$$

can be obtained from the defining equation for G, once the other derivatives are obtained. We have that

$$\frac{\partial^2 G}{\partial v_\perp{}^2} = 2H - \frac{\partial^2 G}{\partial v_\parallel{}^2} - \frac{1}{v_\perp} \frac{\partial G}{\partial v_\perp}, \tag{34}$$

or in the notation introduced here

$$G_{02} = 2H - G_{20} - \frac{G_{01}}{v_\perp}. \tag{35}$$

It is also possible to obtain a convenient elliptic problem for G_{02} by differentiation of (23) with appropriate use of the identity (35). We implement

$$
\frac{\partial^2 G_{02}}{\partial v_\parallel{}^2} + \frac{1}{v_\perp}\frac{\partial}{\partial v_\perp}\left(v_\perp \frac{\partial G_{02}}{\partial v_\perp}\right) - \frac{4G_{02}}{v_\perp^2} = 2\frac{\partial^2 H}{\partial v_\perp{}^2} - \frac{4H}{v_\perp^2} + \frac{2}{v_\perp^2}\frac{\partial^2 G}{\partial v_\parallel{}^2}
$$
$$
= \frac{2}{v_\perp}\frac{\partial}{\partial v_\perp}\left(v_\perp \frac{\partial H}{\partial v_\perp}\right) - \frac{2}{v_\perp}\frac{\partial H}{\partial v_\perp} - \frac{4H}{v_\perp^2} + \frac{2}{v_\perp^2}\frac{\partial^2 G}{\partial v_\parallel{}^2}
\tag{36}
$$

Note that solving for G_{02} requires knowledge of H and other derivatives of G, regardless of the formulation. The primary benefit of using the solution of the elliptic equation (30) rather than the algebraic equation (35) is numerical accuracy.

In analogy to the derivations above, it is straightforward to show that the equations for

$$
H_{10} = \frac{\partial H}{\partial v_\parallel}, \text{ and } H_{01} = \frac{\partial H}{\partial v_\perp}
\tag{37}
$$

are given by

$$
\frac{\partial^2 H_{10}}{\partial v_\parallel{}^2} + \frac{1}{v_\perp}\frac{\partial}{\partial v_\perp}\left(v_\perp \frac{\partial H_{10}}{\partial v_\perp}\right) = -4\pi \frac{\partial F}{\partial v_\parallel}.
\tag{38}
$$

and

$$
\frac{\partial^2 H_{01}}{\partial v_\parallel{}^2} + \frac{1}{v_\perp}\frac{\partial}{\partial v_\perp}\left(v_\perp \frac{\partial H_{01}}{\partial v_\perp}\right) - \frac{H_{01}}{v_\perp^2} = -4\pi \frac{\partial F}{\partial v_\perp},
\tag{39}
$$

respectively. Note that we have written the elliptic equations (26), (30), (32), (36), (38), and (39), in a form that will be amenable to integration by parts in the following test-function analysis required for a weak-form implementation. The numerical implementation of these equations first uses equations (24), (38) and (39) to find H and its derivatives from F. Then, equations (26), (30), (32), and (36) may be solved for the derivatives of G.

2.2. Evaluating the boundary data

Numerical integration of diverging functions is challenging. To obtain the boundary data required to solve the elliptic problems (26), (30), (32), (38), and (39), we aim to avoid Green's functions with denominators that have large powers of g. We can achieve this by using integration by parts to relax the divergence. This has the effect of making the required Green's functions similar in form to those required for G and H.

We start by computing

$$
\frac{\partial G_{s'}}{\partial \mathbf{v}} = \int F_{s'}(\mathbf{v}')\frac{\partial g}{\partial \mathbf{v}} \, d^3\mathbf{v}' = -\int F_{s'}(\mathbf{v}')\frac{\partial g}{\partial \mathbf{v}'} \, d^3\mathbf{v}',
\tag{40}
$$

where we have used that $\partial g/\partial \mathbf{v} = -\partial g/\partial \mathbf{v}'$. Using integration by parts, and that $F_{s'}(\mathbf{v}') \to 0$ as $|\mathbf{v}'| \to 0$, we find that

$$
\frac{\partial G_{s'}}{\partial \mathbf{v}} = \int \frac{\partial F_{s'}}{\partial \mathbf{v}'} g \, d^3\mathbf{v}'.
\tag{41}
$$

We can carry out this procedure a second time to find that

$$\frac{\partial^2 G_{s'}}{\partial \mathbf{v} \partial \mathbf{v}} = \int \frac{\partial^2 F_{s'}}{\partial \mathbf{v'} \partial \mathbf{v'}} g \, d^3 \mathbf{v'}. \tag{42}$$

We can use the same method to find that

$$\frac{\partial H_{s'}}{\partial \mathbf{v}} = \int \frac{\partial F_{s'}}{\partial \mathbf{v'}} \frac{1}{g} \, d^3 \mathbf{v'}. \tag{43}$$

Without the second integration by parts, we also have

$$\frac{\partial^2 G_{s'}}{\partial \mathbf{v} \partial \mathbf{v}} = \int \frac{\partial F_{s'}}{\partial \mathbf{v'}} \frac{\mathbf{v} - \mathbf{v'}}{g} \, d^3 \mathbf{v'}. \tag{44}$$

Equations (41) and (43) are vector equation and (42) and (44) are tensor equations. We extract the relevant coefficients by taking the dot product with the unit vectors $\mathbf{b}$ and $\mathbf{e}_\perp$, noting that

$$\frac{\partial}{\partial \mathbf{v}} = \mathbf{b} \frac{\partial}{\partial v_\parallel} + \mathbf{e}_\perp \frac{\partial}{\partial v_\perp} + \frac{\mathbf{e}_\perp \times \mathbf{b}}{v_\perp} \frac{\partial}{\partial \vartheta}, \tag{45}$$

and

$$\frac{\partial}{\partial \mathbf{v'}} = \mathbf{b} \frac{\partial}{\partial v'_\parallel} + \mathbf{e'}_\perp \frac{\partial}{\partial v'_\perp} + \frac{\mathbf{e'}_\perp \times \mathbf{b}}{v'_\perp} \frac{\partial}{\partial \vartheta'}. \tag{46}$$

Assuming that $F_{s'} = F_{s'}(v'_\parallel, v'_\perp)$ (which implies that $G_{s'} = G_{s'}(v_\parallel, v_\perp)$), we find that

$$\frac{\partial G_{s'}}{\partial v_\perp} = \mathbf{e}_\perp \cdot \frac{\partial G_{s'}}{\partial \mathbf{v}} = \int \frac{\partial F_{s'}}{\partial v'_\perp}(\mathbf{e}_\perp \cdot \mathbf{e'}_\perp) g \, d^3 \mathbf{v'} = 2\pi \int \int \frac{\partial F_{s'}}{\partial v'_\perp} I_{G1} \, v'_\perp dv'_\perp dv'_\parallel, \tag{47}$$

$$\begin{aligned}
\frac{\partial^2 G_{s'}}{\partial v_\parallel \partial v_\perp} &= \mathbf{b}\mathbf{e}_\perp : \frac{\partial^2 G_{s'}}{\partial \mathbf{v} \partial \mathbf{v}} = \int \frac{\partial^2 F_{s'}}{\partial v'_\parallel \partial v'_\perp}(\mathbf{e}_\perp \cdot \mathbf{e'}_\perp) g \, d^3 \mathbf{v'} \\
&= 2\pi \int \int \frac{\partial^2 F_{s'}}{\partial v'_\parallel \partial v'_\perp} I_{G1} \, v'_\perp dv'_\perp dv'_\parallel,
\end{aligned} \tag{48}$$

$$\frac{\partial H_{s'}}{\partial v_\parallel} = \mathbf{b} \cdot \frac{\partial H_{s'}}{\partial \mathbf{v}} = \int \frac{\partial F_{s'}}{\partial v'_\parallel} \frac{1}{g} \, d^3 \mathbf{v'} = 2\pi \int \int \frac{\partial F_{s'}}{\partial v'_\parallel} I_{H0} \, v'_\perp dv'_\perp dv'_\parallel, \tag{49}$$

$$\frac{\partial H_{s'}}{\partial v_\perp} = \mathbf{e}_\perp \cdot \frac{\partial H_{s'}}{\partial \mathbf{v}} = \int \frac{\partial F_{s'}}{\partial v'_\perp} \frac{\mathbf{e}_\perp \cdot \mathbf{e'}_\perp}{g} \, d^3 \mathbf{v'} = 2\pi \int \int \frac{\partial F_{s'}}{\partial v'_\perp} I_{H1} \, v'_\perp dv'_\perp dv'_\parallel. \tag{50}$$

$$\begin{aligned}
\frac{\partial^2 G_{s'}}{\partial v_\parallel{}^2} &= \mathbf{b}\mathbf{b} : \frac{\partial^2 G_{s'}}{\partial \mathbf{v} \partial \mathbf{v}} = \int \frac{\partial F_{s'}}{\partial v'_\parallel} \frac{v_\parallel - v'_\parallel}{g} \, d^3 \mathbf{v'} \\
&= 2\pi \int \int \frac{\partial F_{s'}}{\partial v'_\parallel}(v_\parallel - v'_\parallel) I_{H0} \, v'_\perp dv'_\perp dv'_\parallel,
\end{aligned} \tag{51}$$

and

$$\begin{aligned}
\frac{\partial^2 G_{s'}}{\partial v_\perp{}^2} &= \mathbf{e}_\perp \mathbf{e}_\perp : \frac{\partial^2 G_{s'}}{\partial \mathbf{v} \partial \mathbf{v}} = \int \frac{\partial F_{s'}}{\partial v'_\perp}(\mathbf{e}_\perp \cdot \mathbf{e'}_\perp)\frac{v_\perp - v'_\perp(\mathbf{e}_\perp \cdot \mathbf{e'}_\perp)}{g} \, d^3 \mathbf{v'} \\
&= 2\pi \int \int \frac{\partial F_{s'}}{\partial v'_\perp}(v_\perp I_{H1} - v'_\perp I_{H2}) \, v'_\perp dv'_\perp dv'_\parallel,
\end{aligned} \tag{52}$$

where

$$I_{G1} = \frac{1}{2\pi} \int_{-\pi}^{\pi} g \, (\mathbf{e}_\perp \cdot \mathbf{e}'_\perp) \, d\vartheta', \tag{53}$$

$$I_{H0} = \frac{1}{2\pi} \int_{-\pi}^{\pi} \frac{1}{g} \, d\vartheta', \tag{54}$$

$$I_{H1} = \frac{1}{2\pi} \int_{-\pi}^{\pi} \frac{\mathbf{e}_\perp \cdot \mathbf{e}'_\perp}{g} \, d\vartheta', \tag{55}$$

and

$$I_{H2} = \frac{1}{2\pi} \int_{-\pi}^{\pi} \frac{(\mathbf{e}_\perp \cdot \mathbf{e}'_\perp)^2}{g} \, d\vartheta'. \tag{56}$$

The main advantage of this formulation is that the integrands only diverge logarithmically where $v'_\| = v_\|$ and $v'_\perp = v_\perp$. This kind of divergence can be handled numerically by a change of variables in the affected elements [20]. The functions I_{G1}, I_{H0}, I_{H1}, and I_{H2} are evaluated in Appendix A.

3. Obtaining the weak formulation of the problem

We consider the problem

$$\frac{\partial F}{\partial t} = \frac{\partial \Gamma_\|}{\partial v_\|} + \frac{1}{v_\perp} \frac{\partial}{\partial v_\perp} \left(v_\perp \Gamma_\perp \right). \tag{57}$$

in $v_\| \in [-L_\|, L_\|]$, $v_\perp \in [0, L_\perp]$ and t, where $L_\|$ and $L_\perp$ are the maximum values of $v_\|$ and $v_\perp$ on the grid, respectively. The solution $F = F(v_\|, v_\perp, t)$, and the coefficients $\Gamma_\| = \Gamma_\|(v_\|, v_\perp, t) = \Gamma_\|[F(v_\|, v_\perp, t)]$ and $\Gamma_\perp = \Gamma_\perp(v_\|, v_\perp, t) = \Gamma_\perp[F(v_\|, v_\perp, t)]$ are functionals of F. We note that the fluxes in velocity space are defined explicitly by equations (14) and (15).

We divide the domain into a rectangular grid of $N_{2D} = N_{element,\|} N_{element,\perp}$ elements. We use $N_{element,\|}$ 1D elements in the $v_\|$ direction and $N_{element,\perp}$ 1D elements in the $v_\perp$ direction. Each 2D element is an outer product of two 1D elements. On each 1D element we represent the function with Lagrange polynomials of order $N_{grid} + 1$ using the (normalised) points within the elements

$$x_j \in \{x_0, x_1, ..., x_{N_{grid}-1}, x_{N_{grid}}\} \tag{58}$$

with $x_0 = -1$ and $x_{N_{grid}} = 1$ (Lobatto points) on elements that do not include $v_\perp = 0$. On the element including $v_\perp = 0$, we take $x_{N_{grid}} = 1$ but we use Radau quadrature to ensure that $x_0 > -1$.

The transformation between $(v_\|, v_\perp)$ and the local coordinate $x^{(r)}$ in the rth 1D element is

$$v_\| = s_\|^{(r)} x^{(r)} + c_\|^{(r)}, \quad v_\perp = s_\perp^{(r)} x^{(r)} + c_\perp^{(r)} \tag{59}$$

where $s_\|^{(r)}$, $c_\|^{(r)}$, $s_\perp^{(r)}$ and $c_\perp^{(r)}$ are constants in each element (labelled here by r) which may vary between elements, and $x^{(r)} \in [-1, 1]$ for all r (saving the element including the origin of $v_\perp$, which has $x^{(r)} \in (-1, 1]$).

3.1. The basis functions

We introduce 2D basis functions

$$\Phi_{jk}^{(rp)}\left(v_{\parallel}, v_{\perp}\right) = \varphi_j^{(r)}\left(v_{\parallel}\right)\varphi_k^{(p)}\left(v_{\perp}\right),\tag{60}$$

where the 1D basis functions are

$$\varphi_j^{(r)}\left(v\right) = l_j\left(x^{(r)}\left(v\right)\right) H\left(v - v\left(x_0^{(r)}\right)\right) H\left(v\left(x_{N_{grid}}^{(r)}\right) - v\right),\tag{61}$$

where v is a placeholder for either $v_{\parallel}$ or $v_{\perp}$ and l_j is the jth Lagrange polynomial on the element. Expanding the solution in these basis functions, we write

$$\begin{aligned}
F(v_{\parallel}, v_{\perp}) &= \sum_{r,p}\sum_{j,k} F_{jk}^{rp}\Phi_{jk}^{(rp)}(v_{\parallel}, v_{\perp})\\
&= \sum_{r,p}\sum_{j,k} F_{jk}^{rp}\varphi_j^{(r)}(v_{\parallel})\varphi_k^{(p)}(v_{\perp}),
\end{aligned}\tag{62}$$

with

$$F_{jk}^{rp} = F\left(v_{\parallel}\left(x_j^{(r)}\right), v_{\perp}\left(x_k^{(p)}\right)\right).\tag{63}$$

Note that the basis functions have the cardinality property

$$\varphi_j^{(r)}\left(v\left(x_k^{(p)}\right)\right) = \delta_{jk}\delta_{rp}.\tag{64}$$

3.2. The projection

To project equation (57) onto the basis functions $\Phi_{jk}^{(rp)}\left(v_{\parallel}, v_{\perp}\right)$, we multiply by the basis function $\Phi_{mn}^{(qs)}\left(v_{\parallel}, v_{\perp}\right)$, and integrate over velocity space corresponding to a single 2D element. The limits of this element are $v_{\parallel u}^{(q)} = v_{\parallel}\left(x_{N_{grid}}^{(q)}\right)$, $v_{\parallel l}^{(q)} = v_{\parallel}\left(x_0^{(q)}\right)$, $v_{\perp u}^{(s)} = v_{\perp}\left(x_{N_{grid}}^{(s)}\right)$, and $v_{\perp l}^{(s)} = v_{\perp}\left(x_0^{(s)}\right)$, respectively. Then we have that

$$\int_{v_{\parallel l}^{(q)}}^{v_{\parallel u}^{(q)}} \int_{v_{\perp l}^{(s)}}^{v_{\perp u}^{(s)}} \Phi_{mn}^{(qs)}\frac{\partial F}{\partial t}\, v_{\perp}dv_{\perp}dv_{\parallel} = \int_{v_{\parallel l}^{(q)}}^{v_{\parallel u}^{(q)}} \int_{v_{\perp l}^{(s)}}^{v_{\perp u}^{(s)}} \Phi_{mn}^{(qs)}\left(\frac{\partial \Gamma_{\parallel}}{\partial v_{\parallel}} + \frac{1}{v_{\perp}}\frac{\partial}{\partial v_{\perp}}\left(v_{\perp}\Gamma_{\perp}\right)\right)\, v_{\perp}dv_{\perp}dv_{\parallel}.\tag{65}$$

3.3. The mass matrix

The left hand side of equation (65) takes the form

$$
\int_{v_{\|l}^{(q)}}^{v_{\|u}^{(q)}} \int_{v_{\perp l}^{(s)}}^{v_{\perp u}^{(s)}} \Phi_{mn}^{(qs)} \frac{\partial F}{\partial t} = \sum_{r,p} \sum_{j,k} \frac{\partial F_{jk}^{rp}}{\partial t} \int_{v_{\|l}^{(q)}}^{v_{\|u}^{(q)}} \int_{v_{\perp l}^{(s)}}^{v_{\perp u}^{(s)}} \Phi_{mn}^{(qs)} \Phi_{jk}^{(rp)}\ v_\perp dv_\perp dv_\|
$$

$$
= \sum_{j,k} \frac{\partial F_{jk}^{qs}}{\partial t} \int_{v_{\|l}^{(q)}}^{v_{\|u}^{(q)}} \int_{v_{\perp l}^{(s)}}^{v_{\perp u}^{(s)}} \Phi_{mn}^{(qs)} \Phi_{jk}^{(qs)}\ v_\perp dv_\perp dv_\|
$$

$$
= \sum_{j,k} \frac{\partial F_{jk}^{qs}}{\partial t} \int_{v_{\|l}^{(q)}}^{v_{\|u}^{(q)}} \varphi_m^{(q)}(v_\|)\varphi_j^{(q)}(v_\|)\ dv_\| \int_{v_{\perp l}^{(s)}}^{v_{\perp u}^{(s)}} \varphi_n^{(s)}(v_\perp)\varphi_k^{(s)}(v_\perp)\ v_\perp dv_\perp
$$

$$
= \sum_{j,k} M_{\|mj}^{(q)} M_{\perp nk}^{(s)} \frac{\partial F_{jk}^{qs}}{\partial t}.
$$

$$(66)$$

We deal with the separated integrals as follows

$$
M_{\|mj}^{(q)} = \int_{v_{\|l}^{(q)}}^{v_{\|u}^{(q)}} \varphi_m^{(q)}(v_\|)\varphi_j^{(q)}(v_\|)\ dv_\| = s_\|^{(q)} \int_{-1}^{1} l_m(x)\, l_j(x)\ dx \tag{67}
$$

$$
M_{\perp nk}^{(s)} = \int_{v_{\perp l}^{(s)}}^{v_{\perp u}^{(s)}} \varphi_n^{(s)}(v_\perp)\varphi_k^{(s)}(v_\perp)\ v_\perp dv_\perp = s_\perp^{(s)} \int_{-1}^{1} l_n(x)\, l_k(x)\ \left(s_\perp^{(s)}x + c_\perp^{(s)}\right) dx \tag{68}
$$

The product $M_{\|mj}^{(q)} M_{\perp nk}^{(s)}$ acting on F_{jk}^{rp} is often referred to as a mass matrix.

3.4. The nonlinear stiffness matrices for the collision operator

The form of the right hand side of equation (65) and the forms of the fluxes, given by equations (14) and (15), respectively, suggest that we should integrate by parts to bring all derivatives down to first order. Carrying out this step, we find that for the parallel flux term

$$
\int_{v_{\|l}^{(q)}}^{v_{\|u}^{(q)}} \int_{v_{\perp l}^{(s)}}^{v_{\perp u}^{(s)}} \Phi_{mn}^{(qs)} \frac{\partial \Gamma_\|}{\partial v_\|}\ v_\perp dv_\perp dv_\| = \left[\int_{v_{\perp l}^{(q)}}^{v_{\perp u}^{(q)}} \Phi_{mn}^{(qs)} \Gamma_\|\ v_\perp dv_\perp \right]_{v_{\|l}^{(s)}}^{v_{\|u}^{(s)}} - \int_{v_{\|l}^{(q)}}^{v_{\|u}^{(q)}} \int_{v_{\perp l}^{(s)}}^{v_{\perp u}^{(s)}} \frac{\partial \Phi_{mn}^{(qs)}}{\partial v_\|} \Gamma_\|\ v_\perp dv_\perp dv_\|
$$

$$
= \delta_{mN_{grid}} \int_{v_{\perp l}^{(q)}}^{v_{\perp u}^{(q)}} \Phi_{mn}^{(qs)}(v_{\|u}^{(s)}, v_\perp) \Gamma_\|(v_{\|u}^{(s)}, v_\perp)\ v_\perp dv_\perp
$$

$$
- \delta_{m0} \int_{v_{\perp l}^{(q)}}^{v_{\perp u}^{(q)}} \Phi_{mn}^{(qs)}(v_{\|l}^{(s)}, v_\perp) \Gamma_\|(v_{\|l}^{(s)}, v_\perp)\ v_\perp dv_\perp
$$

$$
- \int_{v_{\|l}^{(q)}}^{v_{\|u}^{(q)}} \int_{v_{\perp l}^{(s)}}^{v_{\perp u}^{(s)}} \frac{\partial \Phi_{mn}^{(qs)}}{\partial v_\|} \Gamma_\|\ v_\perp dv_\perp dv_\|.
$$

$$(69)$$

Similarly, for the perpendicular flux term, we have that

$$
\int_{v_{\|l}^{(q)}}^{v_{\|u}^{(q)}} \int_{v_{\perp l}^{(s)}}^{v_{\perp u}^{(s)}} \frac{\Phi_{mn}^{(qs)}}{v_\perp} \frac{\partial}{\partial v_\perp} \left(v_\perp \Gamma_\perp \right) \, v_\perp dv_\perp dv_\| =
$$

$$
= \int_{v_{\|l}^{(q)}}^{v_{\|u}^{(q)}} \left[\Phi_{mn}^{(qs)} v_\perp \Gamma_\perp \right]_{v_{\perp l}^{(s)}}^{v_{\perp u}^{(s)}} \, dv_\| - \int_{v_{\|l}^{(q)}}^{v_{\|u}^{(q)}} \int_{v_{\perp l}^{(s)}}^{v_{\perp u}^{(s)}} \frac{\partial \Phi_{mn}^{(qs)}}{\partial v_\perp} \Gamma_\perp \, v_\perp dv_\perp dv_\|
$$

$$
= \delta_{nN_{grid}} \int_{v_{\|l}^{(q)}}^{v_{\|u}^{(q)}} \Phi_{mn}^{(qs)}(v_\|, v_{\perp u}^{(s)}) v_{\perp u}^{(s)} \Gamma_\perp(v_\|, v_{\perp u}^{(s)}) \, dv_\| \tag{70}
$$

$$
- \delta_{n0} \int_{v_{\|l}^{(q)}}^{v_{\|u}^{(q)}} \Phi_{mn}^{(qs)}(v_\|, v_{\perp l}^{(s)}) v_{\perp l}^{(s)} \Gamma_\perp(v_\|, v_{\perp l}^{(s)}) \, dv_\|
$$

$$
- \int_{v_{\|l}^{(q)}}^{v_{\|u}^{(q)}} \int_{v_{\perp l}^{(s)}}^{v_{\perp u}^{(s)}} \frac{\partial \Phi_{mn}^{(qs)}}{\partial v_\perp} \Gamma_\perp \, v_\perp dv_\perp dv_\|.
$$

The boundary flux terms in equations (69) and (70) will cancel identically at the assembly stage, or vanish at $v_\perp = 0$ or $v_\perp = L_\perp$, $v_\| = -L_\|$, and $v_\| = L_\|$ by the boundary conditions that $F \to 0$ as $|\mathbf{v}| \to \infty$.

We are now in a position to write down the final matrix row. We use the expansion (62) for both the distribution function F and the coefficients that are derived from the Rosenbluth potentials $G_{s'}$ and $H_{s'}$. With these choices, recalling the definitions of the fluxes $\Gamma_\|$ and $\Gamma_\perp$, equations (14) and (15), respectively, the result is

$$
\sum_{j,k} M_{\|mj}^{(q)} M_{\perp nk}^{(s)} \frac{\partial F_{jk}^{qs}}{\partial t} = -\frac{\gamma_{ss'}}{m_s^2} \sum_{jklr} F_{jk}^{qs} \left(\left[\frac{\partial^2 G_{s'}}{\partial v_\|^2} \right]_{lr}^{(qs)} Y_{\|2mjl}^{(q)} Y_{\perp 0nkr}^{(s)} \right.
$$

$$
+ \left[\frac{\partial^2 G_{s'}}{\partial v_\perp \partial v_\|} \right]_{lr}^{(qs)} Y_{\|1mjl}^{(q)} Y_{\perp 3nkr}^{(s)} - 2\frac{m_s}{m_{s'}} \left[\frac{\partial H_{s'}}{\partial v_\|} \right]_{lr}^{(qs)} Y_{\|1mlj}^{(q)} Y_{\perp 0nkr}^{(s)}
$$

$$
+ \left[\frac{\partial^2 G_{s'}}{\partial v_\perp \partial v_\|} \right]_{lr}^{(qs)} Y_{\|3mjl}^{(q)} Y_{\perp 1nkr}^{(s)} + \left[\frac{\partial^2 G_{s'}}{\partial v_\perp^2} \right]_{lr}^{(qs)} Y_{\|0mjl}^{(q)} Y_{\perp 2nkr}^{(s)}
$$

$$
\left. -2\frac{m_s}{m_{s'}} \left[\frac{\partial H_{s'}}{\partial v_\perp} \right]_{lr}^{(qs)} Y_{\|0mjl}^{(q)} Y_{\perp 1nkr}^{(s)} \right)
$$

$$
+ \delta_{nN_{grid}} \int_{v_{\|l}^{(q)}}^{v_{\|u}^{(q)}} \Phi_{mn}^{(qs)}(v_\|, v_{\perp u}^{(s)}) v_{\perp u}^{(s)} \Gamma_\perp(v_\|, v_{\perp u}^{(s)}) \, dv_\| \tag{71}
$$

$$
- \delta_{n0} \int_{v_{\|l}^{(q)}}^{v_{\|u}^{(q)}} \Phi_{mn}^{(qs)}(v_\|, v_{\perp l}^{(s)}) v_{\perp l}^{(s)} \Gamma_\perp(v_\|, v_{\perp l}^{(s)}) \, dv_\|
$$

$$
+ \delta_{mN_{grid}} \int_{v_{\perp l}^{(s)}}^{v_{\perp u}^{(s)}} \Phi_{mn}^{(qs)}(v_{\|u}^{(q)}, v_\perp) \Gamma_\|(v_{\|u}^{(q)}, v_\perp) \, v_\perp dv_\perp
$$

$$
- \delta_{m0} \int_{v_{\perp l}^{(s)}}^{v_{\perp u}^{(s)}} \Phi_{mn}^{(qs)}(v_{\|l}^{(q)}, v_\perp) \Gamma_\|(v_{\|l}^{(q)}, v_\perp) \, v_\perp dv_\perp,
$$

where we have defined stiffness matrices with three indices

$$Y^{(q)}_{\parallel 0mjl} = \int_{v^{(q)}_{\parallel l}}^{v^{(q)}_{\parallel u}} \varphi^{(q)}_m \varphi^{(q)}_j \varphi^{(q)}_l dv_\parallel, \quad Y^{(q)}_{\parallel 1mjl} = \int_{v^{(q)}_{\parallel l}}^{v^{(q)}_{\parallel u}} \frac{\partial \varphi^{(q)}_m}{\partial v_\parallel} \varphi^{(q)}_j \varphi^{(q)}_l dv_\parallel,$$

$$Y^{(q)}_{\parallel 2mjl} = \int_{v^{(q)}_{\parallel l}}^{v^{(q)}_{\parallel u}} \frac{\partial \varphi^{(q)}_m}{\partial v_\parallel} \frac{\partial \varphi^{(q)}_j}{\partial v_\parallel} \varphi^{(q)}_l dv_\parallel, \quad Y^{(q)}_{\parallel 3mjl} = \int_{v^{(q)}_{\parallel l}}^{v^{(q)}_{\parallel u}} \varphi^{(q)}_m \frac{\partial \varphi^{(q)}_j}{\partial v_\parallel} \varphi^{(q)}_l dv_\parallel, \tag{72}$$

and

$$Y^{(s)}_{\perp 0nkr} = \int_{v^{(s)}_{\perp l}}^{v^{(s)}_{\perp u}} \varphi^{(q)}_n \varphi^{(q)}_k \varphi^{(q)}_r v_\perp \, dv_\perp, \quad Y^{(s)}_{\perp 1nkr} = \int_{v^{(s)}_{\perp l}}^{v^{(s)}_{\perp u}} \frac{\partial \varphi^{(q)}_n}{\partial v_\perp} \varphi^{(q)}_k \varphi^{(q)}_r v_\perp \, dv_\perp,$$

$$Y^{(s)}_{\perp 2nkr} = \int_{v^{(s)}_{\perp l}}^{v^{(s)}_{\perp u}} \frac{\partial \varphi^{(q)}_n}{\partial v_\perp} \frac{\partial \varphi^{(q)}_k}{\partial v_\perp} \varphi^{(q)}_r v_\perp \, dv_\perp, \quad Y^{(s)}_{\perp 3nkr} = \int_{v^{(s)}_{\perp l}}^{v^{(s)}_{\perp u}} \varphi^{(q)}_n \frac{\partial \varphi^{(q)}_k}{\partial v_\perp} \varphi^{(q)}_r v_\perp \, dv_\perp. \tag{73}$$

Note that the stiffness matrices in (71) are all 1D integrals of 1D basis functions, as a result of the choice to use the representation (62) where the 2D basis function $\Phi^{(qs)}_{mn}(v_\parallel, v_\perp)$ is a product of two 1D lagrange polynomials – one for the $v_\parallel$ dimension, and one for the $v_\perp$ dimension.

The assembly step is carried out by defining a compound index that indexes over all the rows in $(v_\parallel, v_\perp)$, and then forming a matrix equation in that index. We use continuity of F to demand that $F^{q,s}_{jN_{grid}} = F^{q,s+1}_{j0}$, $F^{q,s}_{N_{grid}k} = F^{q+1,s}_{0k}$, and remove the duplicated points at interior element boundaries by summing the matrix rows there.

3.5. The weak form of the equations for the Rosenbluth potentials

We still need to determine the coefficients derived from the Rosenbluth potentials. We start by considering the solution of Poisson's equation, equation (24). Multiplying by the 2D basis function $\Phi^{(rp)}_{jk} = \varphi^{(r)}_j (v_\parallel) \varphi^{(p)}_k (v_\perp)$ and integrating over velocity space we have

$$-\int\int \Phi^{(rp)}_{jk} \left(\frac{\partial^2 H}{\partial v_\parallel^2} + \frac{1}{v_\perp} \frac{\partial}{\partial v_\perp} \left(v_\perp \frac{\partial H}{\partial v_\perp} \right) \right) v_\perp \, dv_\perp \, dv_\parallel = -4\pi \int\int F v_\perp \, dv_\perp \, dv_\parallel. \tag{74}$$

Integrating by parts and neglecting the boundary terms (which either vanish or will be cancelled at the assembly step) we have that

$$\int\int \left(\frac{\partial \Phi^{(rp)}_{jk}}{\partial v_\parallel} \frac{\partial H}{\partial v_\parallel} + \frac{\partial \Phi^{(rp)}_{jk}}{\partial v_\perp} \frac{\partial H}{\partial v_\perp} \right) v_\perp \, dv_\perp \, dv_\parallel = -4\pi \int\int F v_\perp \, dv_\perp \, dv_\parallel. \tag{75}$$

Defining the matrices

$$K^{(s)}_{\perp nk} = -\int_{v^{(s)}_{\perp l}}^{v^{(s)}_{\perp u}} \frac{\partial \varphi^{(s)}_n}{\partial v_\perp} \frac{\partial \varphi^{(s)}_k}{\partial v_\perp} v_\perp dv_\perp \tag{76}$$

and

$$K^{(s)}_{\parallel nk} = -\int_{v^{(s)}_{\parallel l}}^{v^{(s)}_{\parallel u}} \frac{\partial \varphi^{(s)}_n}{\partial v_\parallel} \frac{\partial \varphi^{(s)}_k}{\partial v_\parallel} dv_\parallel \tag{77}$$

and expanding

$$F = \sum_{rp} \sum_{jk} \Phi_{jk}^{(rp)} F_{jk}^{rp}, \quad H = \sum_{rp} \sum_{jk} \Phi_{jk}^{(rp)} H_{jk}^{rp}, \tag{78}$$

we find that the row of the unassembled matrix is

$$\sum_{mn} \left(K_{\|jm}^{(r)} M_{\perp kn}^{(p)} + K_{\perp kn}^{(p)} M_{\|jm}^{(r)} \right) H_{mn}^{rp} = -4\pi \sum_{mn} M_{\|jm}^{(r)} M_{\perp kn}^{(p)} F_{mn}^{rp}. \tag{79}$$

We impose Dirichlet boundary conditions on the assembled matrices using the exact values of the required functions. Once the coefficients H_{jk}^{rp} are known then the same matrices can be used in an identical fashion to solve for G_{jk}^{rp}. A similar matrix equation can be written down to solve for G_{20jk}^{rp} and H_{10jk}^{rp}, with the only difference being in the source terms on the right-hand side. Explicitly, these results are

$$\sum_{mn} \left(K_{\|jm}^{(r)} M_{\perp kn}^{(p)} + K_{\perp kn}^{(p)} M_{\|jm}^{(r)} \right) H_{01mn}^{rp} = -4\pi \sum_{mn} P_{\|jm}^{(r)} M_{\perp kn}^{(p)} F_{mn}^{rp}. \tag{80}$$

where we have defined

$$P_{\|mj}^{(r)} = \int_{v_{\perp l}^{(r)}}^{v_{\perp u}^{(r)}} \varphi_m^{(r)} \frac{\partial \varphi_j^{(r)}}{\partial v_{\|}} \, dv_{\|}, \tag{81}$$

and

$$\sum_{mn} \left(K_{\|jm}^{(r)} M_{\perp kn}^{(p)} + K_{\perp kn}^{(p)} M_{\|jm}^{(r)} \right) G_{mn}^{rp} = 2 \sum_{mn} M_{\|jm}^{(r)} M_{\perp kn}^{(p)} H_{mn}^{rp}. \tag{82}$$

Note that a double Poisson solve is required to obtain G from F. We choose to find $\partial H / \partial v_{\|}$ by a separate Poisson solve rather than differentiating H to improve numerical accuracy.

To find the equations for the other coefficients in the fluxes, we must repeat the exercise above. The PDE defining $G_{01} = \partial G / \partial v_{\perp}$ is distinct from Poisson's equation and will require different matrix elements on the left-hand side. We again start by multiplying equation (30) by the function $v_{\perp}^2 \Phi_{jk}^{(rp)}$, we find that

$$\int \int v_{\perp}^2 \Phi_{jk}^{(rp)} \left(\frac{\partial^2 G_{01}}{\partial v_{\|}^2} + \frac{1}{v_{\perp}} \frac{\partial}{\partial v_{\perp}} \left(v_{\perp} \frac{\partial G_{01}}{\partial v_{\perp}} \right) - \frac{G_{01}}{v_{\perp}^2} \right) \, dv_{\perp} \, dv_{\|}$$
$$= 2 \int \int v_{\perp}^2 \frac{\partial H}{\partial v_{\perp}} \, dv_{\perp} \, dv_{\|}. \tag{83}$$

Integrating by parts, expanding the derivatives, and neglecting boundary terms, we find that

$$-\int \int \left(v_{\perp}^2 \frac{\partial \Phi_{jk}^{(rp)}}{\partial v_{\|}} \frac{\partial G_{01}}{\partial v_{\|}} + v_{\perp}^2 \frac{\partial G_{01}}{\partial v_{\perp}} \frac{\partial \Phi_{jk}^{(rp)}}{\partial v_{\perp}} + v_{\perp} \Phi_{jk}^{(rp)} \frac{\partial G_{01}}{\partial v_{\perp}} + \Phi_{jk}^{(rp)} G_{01} \right) \, dv_{\perp} \, dv_{\|}$$
$$= 2 \int \int v_{\perp}^2 \frac{\partial H}{\partial v_{\perp}} \, dv_{\perp} \, dv_{\|}. \tag{84}$$

Expanding $G_{01} = \sum_{rp} \sum_{mn} \Phi_{mn}^{(rp)} G_{01mn}^{rp}$ we thus find the unassembled matrix row

$$-\sum_{mn} G_{01mn}^{rp} \int \int \left(v_\perp^2 \frac{\partial \Phi_{jk}^{(rp)}}{\partial v_\parallel} \frac{\partial \Phi_{mn}^{(rp)}}{\partial v_\parallel} + v_\perp^2 \frac{\partial \Phi_{mn}^{(rp)}}{\partial v_\perp} \frac{\partial \Phi_{jk}^{(rp)}}{\partial v_\perp} + v_\perp \Phi_{jk}^{(rp)} \frac{\partial \Phi_{mn}^{(rp)}}{\partial v_\perp} + \Phi_{jk}^{(rp)} \Phi_{mn}^{(rp)} \right) \, dv_\perp \, dv_\parallel$$

$$= 2\sum_{mn} H_{mn}^{rp} \int \int v_\perp^2 \Phi_{jk}^{(rp)} \frac{\partial \Phi_{mn}^{(rp)}}{\partial v_\perp} \, dv_\perp \, dv_\parallel. \tag{85}$$

If we define the matrix elements

$$R_{\perp nk}^{(s)} = \int_{v_{\perp l}^{(s)}}^{v_{\perp u}^{(s)}} \varphi_n^{(s)}(v_\perp) \varphi_k^{(s)}(v_\perp) \, v_\perp^2 dv_\perp, \quad N_{\perp nk}^{(s)} = \int_{v_{\perp l}^{(s)}}^{v_{\perp u}^{(s)}} \varphi_n^{(s)}(v_\perp) \varphi_k^{(s)}(v_\perp) \, dv_\perp,$$

$$J_{\perp nk}^{(s)} = -\int_{v_{\perp l}^{(s)}}^{v_{\perp u}^{(s)}} \frac{\partial \varphi_n^{(s)}}{\partial v_\perp} \frac{\partial \varphi_k^{(s)}}{\partial v_\perp} \, v_\perp^2 dv_\perp, \quad P_{\perp nk}^{(s)} = \int_{v_{\perp l}^{(s)}}^{v_{\perp u}^{(s)}} \varphi_n^{(s)} \frac{\partial \varphi_k^{(s)}}{\partial v_\perp} \, v_\perp dv_\perp, \tag{86}$$

and

$$U_{\perp nk}^{(s)} = \int_{v_{\perp l}^{(s)}}^{v_{\perp u}^{(s)}} \varphi_n^{(s)} \frac{\partial \varphi_k^{(s)}}{\partial v_\perp} \, v_\perp^2 dv_\perp \tag{87}$$

then we can write the row as

$$\sum_{mn} \left(K_{\parallel jm}^{(r)} R_{\perp kn}^{(p)} + M_{\parallel jm}^{(r)} J_{\perp kn}^{(p)} - M_{\parallel jm}^{(r)} P_{\perp kn}^{(p)} - M_{\parallel jm}^{(r)} N_{\perp kn}^{(p)} \right) G_{01mn}^{rp}$$

$$= 2\sum_{mn} M_{\parallel jm}^{(r)} U_{\perp kn}^{(p)} H_{mn}^{rp}. \tag{88}$$

The PDE for $G_{11} = \partial^2 G / \partial v_\parallel \partial v_\perp$ is identical to the one for G_{01} apart from the right-hand side. We obtain the weak form

$$-\int \int \left(v_\perp^2 \frac{\partial \Phi_{jk}^{(rp)}}{\partial v_\parallel} \frac{\partial G_{11}}{\partial v_\parallel} + v_\perp^2 \frac{\partial G_{11}}{\partial v_\perp} \frac{\partial \Phi_{jk}^{(rp)}}{\partial v_\perp} + v_\perp \Phi_{jk}^{(rp)} \frac{\partial G_{11}}{\partial v_\perp} + \Phi_{jk}^{(rp)} G_{11} \right) \, dv_\perp \, dv_\parallel$$

$$= 2\int \int v_\perp^2 \frac{\partial^2 H}{\partial v_\parallel \partial v_\perp} \, dv_\perp \, dv_\parallel. \tag{89}$$

The corresponding matrix row is

$$\sum_{mn} \left(K_{\parallel jm}^{(r)} R_{\perp kn}^{(p)} + M_{\parallel jm}^{(r)} J_{\perp kn}^{(p)} - M_{\parallel jm}^{(r)} P_{\perp kn}^{(p)} - M_{\parallel jm}^{(r)} N_{\perp kn}^{(p)} \right) G_{11mn}^{rp}$$

$$= 2\sum_{mn} P_{\parallel jm}^{(r)} U_{\perp kn}^{(p)} H_{mn}^{rp}. \tag{90}$$

Similarly, the PDE for H_{01}, equation (39) has the weak form

$$\sum_{mn} \left(K_{\parallel jm}^{(r)} R_{\perp kn}^{(p)} + M_{\parallel jm}^{(r)} J_{\perp kn}^{(p)} - M_{\parallel jm}^{(r)} P_{\perp kn}^{(p)} - M_{\parallel jm}^{(r)} N_{\perp kn}^{(p)} \right) H_{01mn}^{rp}$$

$$= -4\pi \sum_{mn} M_{\parallel jm}^{(r)} U_{\perp kn}^{(p)} F_{mn}^{rp}. \tag{91}$$

To complete the set of coefficients, we can either use the algebraic equation (35) or the elliptic problem (36) for $G_{02} = \partial^2 G / \partial v_\perp{}^2$. First considering equation (35) and projecting on to the basis functions, we have that

$$\int\int \Phi_{jk}^{(rp)} G_{02}\, v_\perp dv_\perp dv_\parallel = \int\int \Phi_{jk}^{(rp)}\left(v_\perp(2H - G_{20}) - G_{01}\right)\, dv_\perp dv_\parallel. \tag{92}$$

The corresponding matrix row therefore becomes

$$\sum_{mn} M_{\parallel jm}^{(r)} M_{\perp kn}^{(p)} G_{02mn}^{rp} = \sum_{mn} M_{\parallel jm}^{(r)} M_{\perp kn}^{(p)} (2H_{mn}^{rp} - G_{20mn}^{rp}) - M_{\parallel jm}^{(r)} N_{\perp kn}^{(p)} G_{01mn}^{rp}. \tag{93}$$

Secondly, considering equation (36), we have the weak-form

$$-\int\int \left(v_\perp^2 \frac{\partial \Phi_{jk}^{(rp)}}{\partial v_\parallel} \frac{\partial G_{02}}{\partial v_\parallel} + v_\perp^2 \frac{\partial \Phi_{jk}^{(rp)}}{\partial v_\perp} \frac{\partial G_{02}}{\partial v_\perp} - v_\perp \Phi_{jk}^{(rp)} \frac{\partial G_{02}}{\partial v_\perp} - 4\Phi_{jk}^{(rp)} G_{02} \right)\, dv_\perp dv_\parallel$$

$$= -\int\int \left(v_\perp^2 \frac{\partial \Phi_{jk}^{(rp)}}{\partial v_\perp} \frac{\partial H}{\partial v_\perp} + 2v_\perp \Phi_{jk}^{(rp)} \frac{\partial H}{\partial v_\perp} + 2\Phi_{jk}^{(rp)} H \right)\, dv_\perp dv_\parallel + \int\int \Phi_{jk}^{(rp)} G_{20}\, dv_\perp dv_\parallel, \tag{94}$$

where we have carried out the integration by parts and neglected to write boundary terms. The corresponding row of the unassembled matrix therefore becomes

$$\sum_{mn} \left(K_{\parallel jm}^{(r)} R_{\perp kn}^{(p)} + M_{\parallel jm}^{(r)} (J_{\perp kn}^{(p)} - P_{\perp kn}^{(p)} - 4N_{\perp kn}^{(p)}) \right) G_{02mn}^{rp}$$

$$= 2\left(\sum_{mn} M_{\parallel jm}^{(r)} (J_{\perp kn}^{(p)} - 2P_{\perp kn}^{(p)} - N_{\perp kn}^{(p)}) H_{mn}^{rp} - 2 \sum_{mn} M_{\parallel jm}^{(r)} N_{\perp kn}^{(p)} G_{20mn}^{rp} \right). \tag{95}$$

3.6. Velocity space integration in the spectral element scheme

To compute the boundary data for the elliptic solvers obtained in the last section, we need to integrate a function $F = F(v_\parallel', v_\perp')$ multiplied by a kernel function

$$\mathcal{G} = \mathcal{G}(v_\parallel, v_\perp, v_\parallel', v_\perp'), \tag{96}$$

i.e., we wish to compute

$$I = \int_{-\infty}^{\infty} \int_0^{\infty} \mathcal{G}(v_\parallel, v_\perp, v_\parallel', v_\perp') F(v_\parallel', v_\perp') v_\perp' dv_\perp' dv_\parallel'. \tag{97}$$

We expand F in the Lagrange polynomial basis functions using equation (62) and thus obtain that

$$I = \sum_{rp} \sum_{jk} F_{jk}^{rp} I_{jk}^{(rp)} \tag{98}$$

with the integration over local elements

$$I_{jk}^{(rp)} = \int_{v_{\parallel l}^{(r)}}^{v_{\parallel u}^{(r)}} \int_{v_{\perp l}^{(p)}}^{v_{\perp u}^{(p)}} \mathcal{G}(v_\parallel, v_\perp, v_\parallel', v_\perp') \varphi_j^{(r)}(v_\parallel') \varphi_k^{(p)}(v_\perp') v_\perp' dv_\perp' dv_\parallel'. \tag{99}$$

When assembling the element problem, one must recall that at element boundaries the nodal value of F has an interpolating polynomial that should be integrated over on both elements.

4. Boundary conditions for time evolution

The collision operator described in this report is intended to be used alongside explicit pseudo-spectral advection terms in both space and velocities. As such, boundary conditions are imposed explicitly at the boundaries of the domain each time step, by explicitly forcing the appropriate conditions on F_s.

In the assembly of the collision operator (71), we imposed a "zero-flux" boundary condition $\Gamma_\parallel(v_\parallel = \pm L_\parallel) = \Gamma_\perp(v_\perp = L_\perp) = 0$ by virtue of neglecting the boundary fluxes in the implementation. However, for the advection terms, we must impose $F_s = 0$ at the upwind boundaries of velocity space. For physical solutions we would expect $F_s = 0$ and the "zero-flux" boundary conditions to be equivalent.

The use of cylindrical coordinates introduces a spurious boundary into the coordinate system at $v_\perp = 0$. To ensure regularity of the solution at $v_\perp = 0$, we impose

$$\left.\frac{\partial F_s}{\partial v_\perp}\right|_{v_\perp=0} = 0. \tag{100}$$

We motivate this by noting that for $F_s = F_s(\mathbf{v})$ to be continuous and differentiable as a function of the vector velocity argument $\mathbf{v}$ near $\mathbf{v} = 0$, then (100) must be satisfied.

5. Ad-hoc numerical conserving terms

The numerical scheme here is chosen for speed and accuracy rather than for exact satisfaction of the necessary conservative properties (5)-(7). To ensure that the numerical scheme also preserves the density, parallel velocity and pressure at each time step (to machine precision), for time-evolving simulations we introduce ad-hoc conserving terms which make a correction which is (in principle) of order the discretisation error. Noting the definitions of the plasma density n_s and parallel flow $u_{\parallel,s}$,

$$n_s = \int\int F_s \, 2\pi v_\perp dv_\perp \, dv_\parallel, \tag{101}$$

and

$$n_s u_{\parallel,s} = \int\int v_\parallel F_s \, 2\pi v_\perp dv_\perp \, dv_\parallel, \tag{102}$$

respectively, we define

$$C_{ss}\left[F_s, F_s\right] = C_{ss}^*\left[F_s, F_s\right] - \left(x_0 + x_1(v_\parallel - u_{\parallel,s}) + x_2\left((v_\parallel - u_{\parallel,s})^2 + v_\perp^2\right)\right)F_s, \tag{103}$$

where $C_{ss}^*\left[F_s, F_s\right]$ denotes the numerically calculated finite-element collision operator given by $\partial F/\partial t$ in equation (71), and the coefficients x_0, x_1 and x_2 are determined by the requirements that (5)-(7) are exactly satisfied. These requirements lead to the matrix equation

$$\begin{pmatrix} n_s & 0 & 3p_s \\ 0 & p_{\parallel,s} & q_{\parallel,s} \\ 3p_s & q_{\parallel,s} & \tilde{R}_s \end{pmatrix} \begin{pmatrix} x_0 \\ x_1 \\ x_2 \end{pmatrix} = \begin{pmatrix} \Delta n_s \\ n_s\Delta u_{\parallel,s} - u_{\parallel,s}\Delta n_s \\ 3\Delta p_s \end{pmatrix} \tag{104}$$

where the vector components on the right hand side are the moments of $C_{ss}^*[F_s, F_s]$

$$\Delta n_s = \int \int C_{ss}^*[F_s, F_s] \; 2\pi v_\perp dv_\perp dv_\parallel,$$

$$\Delta u_{\parallel,s} = \frac{1}{n_s} \int \int v_\parallel C_{ss}^*[F_s, F_s] \; 2\pi v_\perp dv_\perp dv_\parallel, \text{and} \tag{105}$$

$$\Delta p_s = \frac{1}{3} \int \int \left((v_\parallel - u_{\parallel,s})^2 + v_\perp^2 \right) C_{ss}^*[F_s, F_s] \; 2\pi v_\perp dv_\perp dv_\parallel,$$

and the compoments of the matrix on the left-hand side are given by the moments of F_s. We have that the total pressure $p_s = (2p_{\perp,s} + p_{\parallel,s})/3$ with the parallel and perpendicular pressures given by

$$p_{\parallel,s} = \int \int (v_\parallel - u_{\parallel,s})^2 F_s \; 2\pi v_\perp dv_\perp \; dv_\parallel, \tag{106}$$

and

$$p_{\perp,s} = \frac{1}{2} \int \int v_\perp^2 F_s \; 2\pi v_\perp dv_\perp \; dv_\parallel, \tag{107}$$

respectively. The parallel heat flux is given by

$$q_{\parallel,s} = \int \int (v_\parallel - u_{\parallel,s})((v_\parallel - u_{\parallel,s})^2 + v_\perp^2) F_s \; 2\pi v_\perp dv_\perp \; dv_\parallel, \tag{108}$$

and the higher-order moment

$$\tilde{R}_s = \int \int ((v_\parallel - u_{\parallel,s})^2 + v_\perp^2)^2 F_s \; 2\pi v_\perp dv_\perp \; dv_\parallel. \tag{109}$$

To achieve good results with this method, the boundary conditions that are imposed on F_s should also be imposed on $C_{ss}^*[F_s, F_s]$ before evaluating the values of the set of coefficients $\{x_i\}$.

We note the similarity of these ad-hoc conserving terms to those employed for similar reasons where the density, parallel flow, and pressure are required to be conserved exactly [10, 21].

6. Numerical implementation and results

We have implemented an explicit form of the weak-form collision operator in a script to test the numerical properties, as well as in the main time-advance loop of "moment_kinetics". Specifically, we have implemented the assembled weak-form problems defined by equations (71), (79), (80), (82), (88), (90), (91), (95), using sparse matrices `https://docs.julialang.org/en/v1/stdlib/SparseArrays/`, using the "moment kinetics" shared-memory MPI, with appropriate calculations of the boundary data using the integration weights defined by (99). We use Gauss-Legendre polynomials to define the Lobatto and Radau collocation grid points. We have implemented the scheme for arbitrary order of polynomial. The implementation may be found in the branch at the following URL `https://`

github.com/mabarnes/moment_kinetics/tree/merge_fkpl_collisions. The software required to execute the tests described in section 6.1 are contained in the test script in the following URL https://github.com/mabarnes/moment_kinetics/tree/merge_fkpl_collisions/test_scripts/2D_FEM_assembly_test.jl, on commit c24dbc6. This relaxation test described in section 6.2 uses an input file based on https://github.com/mabarnes/moment_kinetics/blob/merge_fkpl_collisions/examples/fokker-planck/fokker-planck-relaxation.toml.

6.1. Evaluation tests

We wish to test the three properties of the collision operator (5)-(7). To facilitate this test we define three quantities which measure the change in the moments of the distribution function due to the collision operator, given by equation (105). We test whether or not the collision operator vanishes on a prescribed Maxwellian distribution, i.e.,

$$C_{ss}\left[F_s^M, F_s^M\right] = 0, \tag{110}$$

as a proxy for testing the entropy production inequality (8). In figures 1, 2, 3, and 4, we carry out the test on 2 cores for varying $N_{element}$ at fixed $N_{grid} = 3, 5, 7,$ and 9, respectively. Here $N_{element}$ is the number of elements in the $v_\perp$ dimension and half the number of elements in the $v_\parallel$ dimension. The quantity N_{grid} is the number of points per element. We take the maximum velocity to be $L_\parallel = L_\perp = 6.0$. Note that reducing the maximum $v_\parallel$ and $v_\perp$ on the grids for a fixed integrand reduces the accuracy of the numerical integration because the true velocity integrals should extend to infinite velocities. We choose to carry out the test with a Maxwellian with a normalised density $n_s/n_{\mathrm{ref}} = 1.0$, a normalised $u_{\parallel,s}/c_{\mathrm{ref}} = 1.0$, with $c_{\mathrm{ref}} = \sqrt{2T_{\mathrm{ref}}/m_{\mathrm{ref}}}$ and a normalised $T_s/T_{\mathrm{ref}} = 1.0$.

In the figure (a) of figures 1-4, we plot both the infinity norm of the error ϵ_∞ and the L_2 norm of the error ϵ_{L_2} of calculating the collision operator with respect to the expected value (which is zero). We see that the infinity norm gives a larger value than the L_2 norm in all cases by a factor of an order of magnitude. This is due to numerical oscillations near $v_\perp = 0$ where the differential equations become singular. For $N_{grid} = 3$ (quadratic interpolating polynomials) the error in computing the collision operator does not decrease rapidly with $N_{element}$, but the error does follow the expected scaling for differentiation

$$\left(\frac{1}{N_{element}}\right)^{N_{grid}-1}. \tag{111}$$

However, the quantities Δn_s, $\Delta u_{\parallel,s}$, and Δp_s approach zero rapidly at (or better than) the expected scaling for numerical integration errors

$$\left(\frac{1}{N_{element}}\right)^{N_{grid}+1}. \tag{112}$$

This picture becomes clearer for larger N_{grid}, as evidenced in figures 2-4.

To demonstrate the attained performance of the explicit collision operator, in figure (b) of figures 1-4, we plot the timing data (in milli seconds) for completing the initialisation and evaluation of the collision operator. The expected scaling for the initialisation is $N^3_{element}$, by virtue of the calculation of the integration weights for the boundary data. The expected scaling for the evaluation of the collision operator depends on which operation dominates the calculation. If it is the computation of the boundary data it is $N^3_{element}$, whereas if it is the elliptic solve or the assembly of the right hand side of equation (71) then the scaling would be expected to be $N^2_{element}$ due to the sparse nature of these operations. In figure 1b for $N_{grid} = 3$ the timing for both the initialisation and single evaluation scales like $N^3_{element}$, whereas, in figures 2b-4b for $N_{grid} = 5$-9, respectively, we see that a scaling closer to $N^2_{element}$ is acheived for the evaluation step. This is promising for the scaling of the operator to large problem sizes.

To understand the dominant source of the numerical error, we find it useful to plot the infinity and L_2 norm error measures of the numerically calculated Rosenbluth potential coefficients $\partial H/\partial v_\parallel$, $\partial H/\partial v_\perp$, $\partial^2 G/\partial v_\parallel{}^2$, $\partial G/\partial v_\perp$, $\partial^2 G/\partial v_\parallel \partial v_\perp$, and $\partial^2 G/\partial v_\perp{}^2$. The exact values are known and may be computed easily for shifted Maxwellian distributions [22]. We plot this data for $N_{grid} = 3$ in figure 5, and for $N_{grid} = 9$ in in figure 6. We see that for both $N_{grid} = 3$ and $N_{grid} = 9$, the L_2 norm error is smaller by one or two orders of magnitude than the infinity norm error. This is due to numerical oscillations near $v_\perp = 0$. However, in both cases the errors decay to zero at least at the rate given by equation (111) (for $N_{grid} = 3$), or at the proper expected rate given by equation (112) (for $N_{grid} = 9$). Note that our numerical calculation of the boundary data does involve a numerical differentiation of F, see equations (47)-(52). In the case of $N_{grid} = 9$, we see that the errors deviate from the scaling for high resolution, which we take to mean that we have reached the smallest error possible with double floating point precision. We take this to indicate that the dominant source of numerical error in evaluating the collision operator in fact comes from the unavoidable numerical differentiation, rather than from the errors in obtaining the Rosenbluth potential coefficients. Indeed, comparable levels of error to that seen in computing the collision operator may be obtained by simply using the weak method to differentiate F to find the second derivatives in $v_\parallel$ and $v_\perp$.

6.2. Relaxation to a Maxwellian distribution: testing equation (8)

It is important to test whether or not the numerical self-collision operator can provide a stable, steady-state numerical solution which is close to a Maxwellian distribution, whilst satisfying equation (8). Using the ad-hoc numerically conserving model (103), we find that we can obtain a stable solution even for very low numerical resolution. In figure 7, we show time traces of the change in the density, parallel flow and pressure over the course of the simulation. In figure 8 we show the entropy production, calculated using the definition (8) and using the following approximation for the logarithm of the
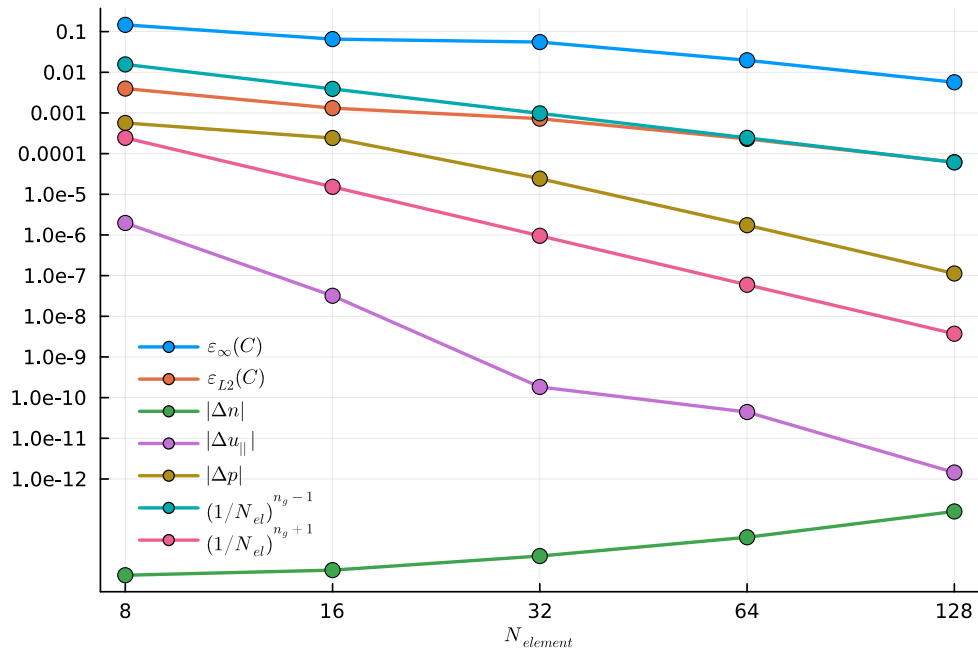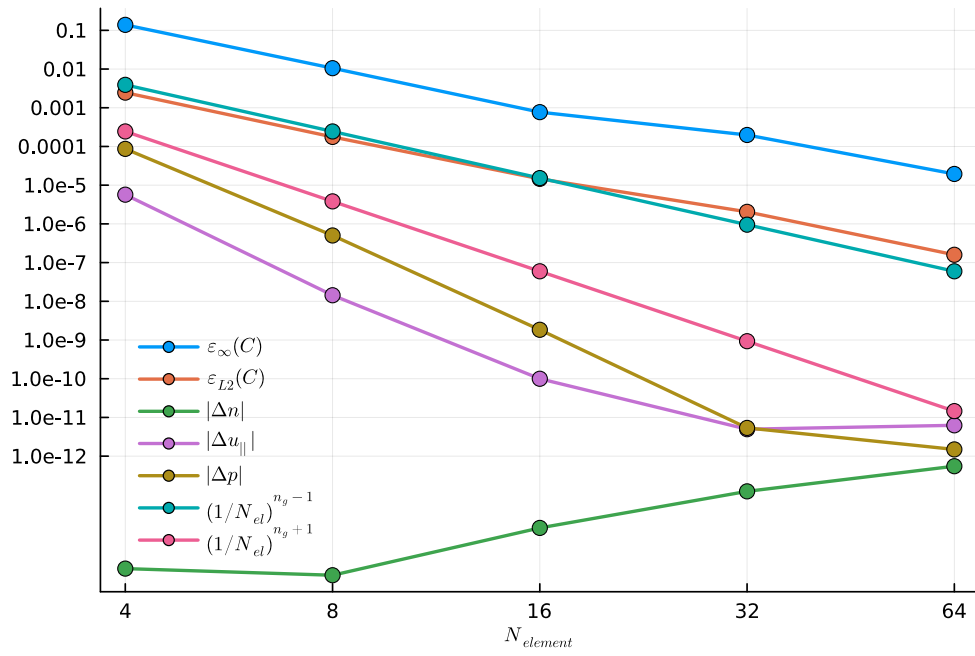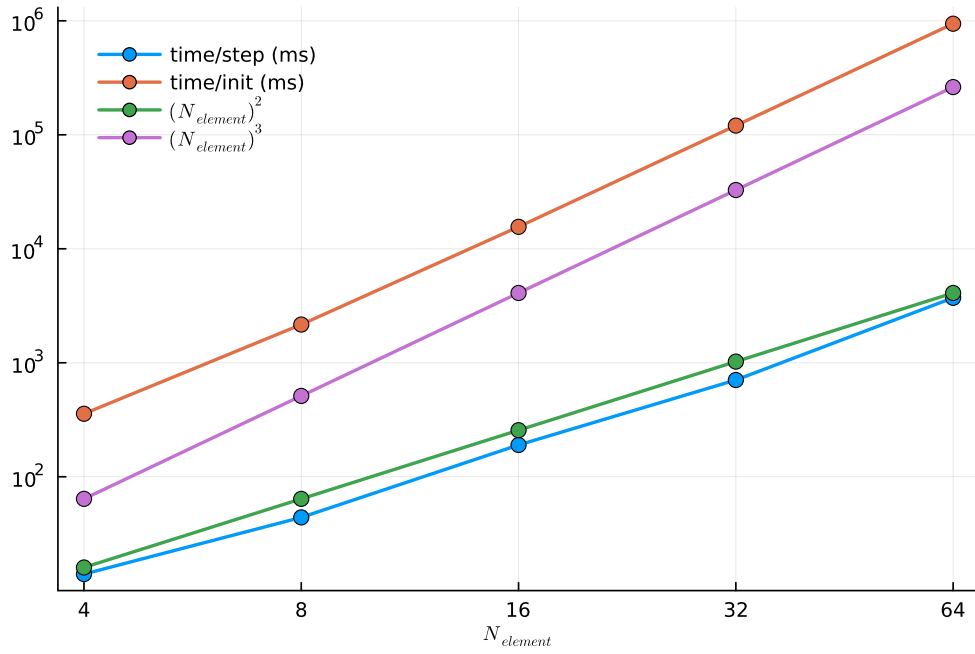
(a)
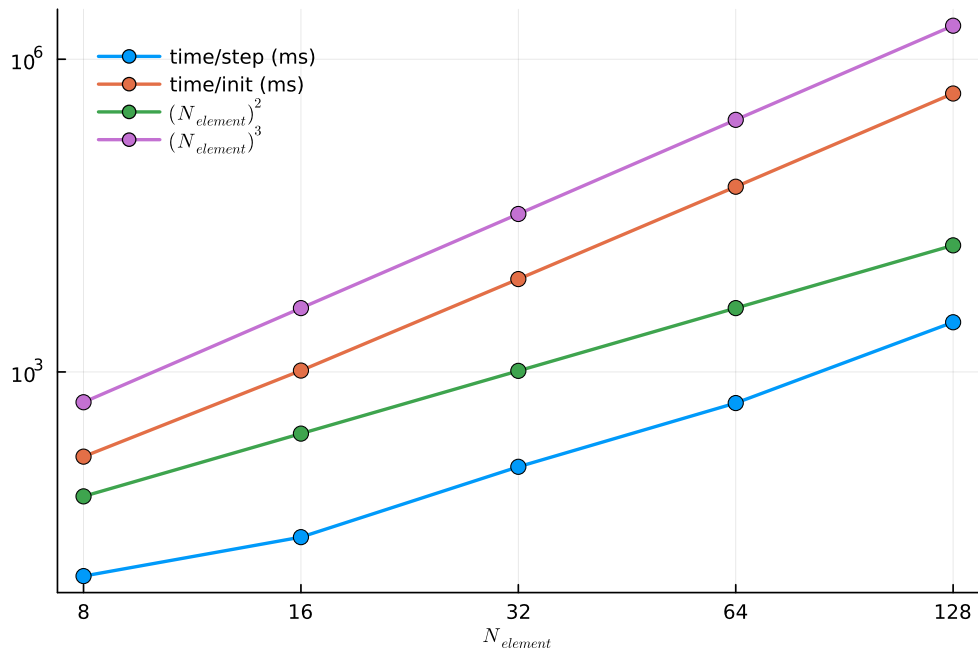
(b)

Figure 1: The numerical error and timing data for the test carried out on 2 cores with $N_{grid} = n_g = 3$ points per element. The infinity and L_2 norms of the collision operator are shown and compared to the expected scalings for differentiation and integration (111) and (112), respectively. The timing data for the initialisation (init) and a single evaluation of the collision operator (step) is given in milliseconds.
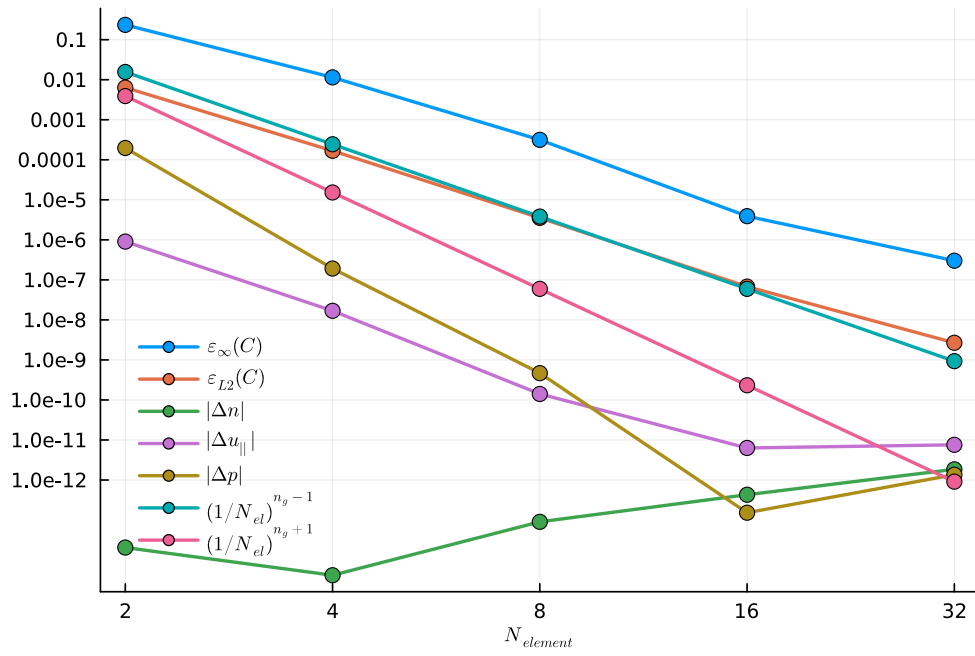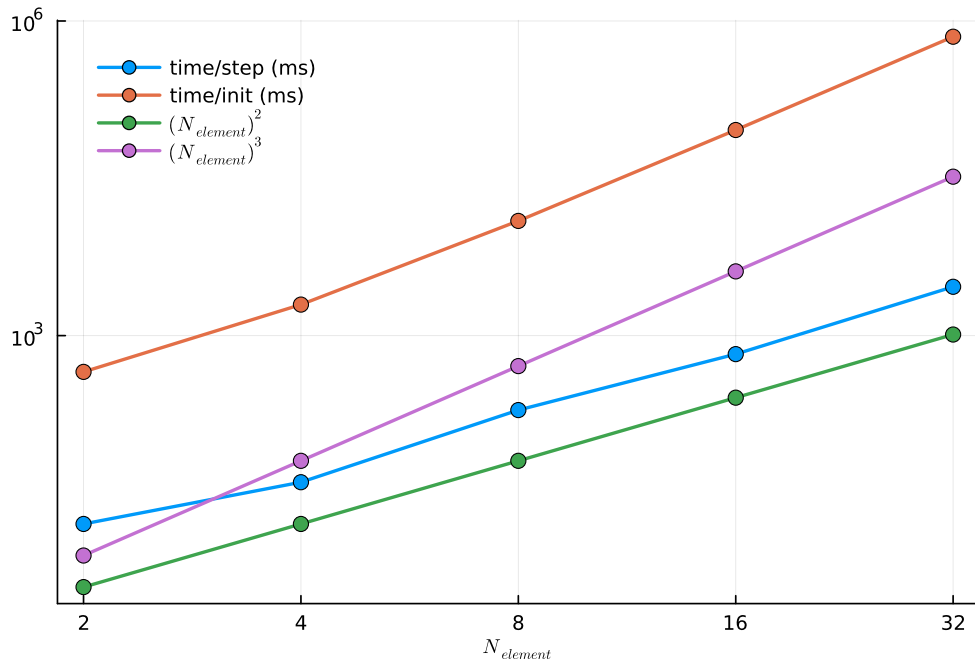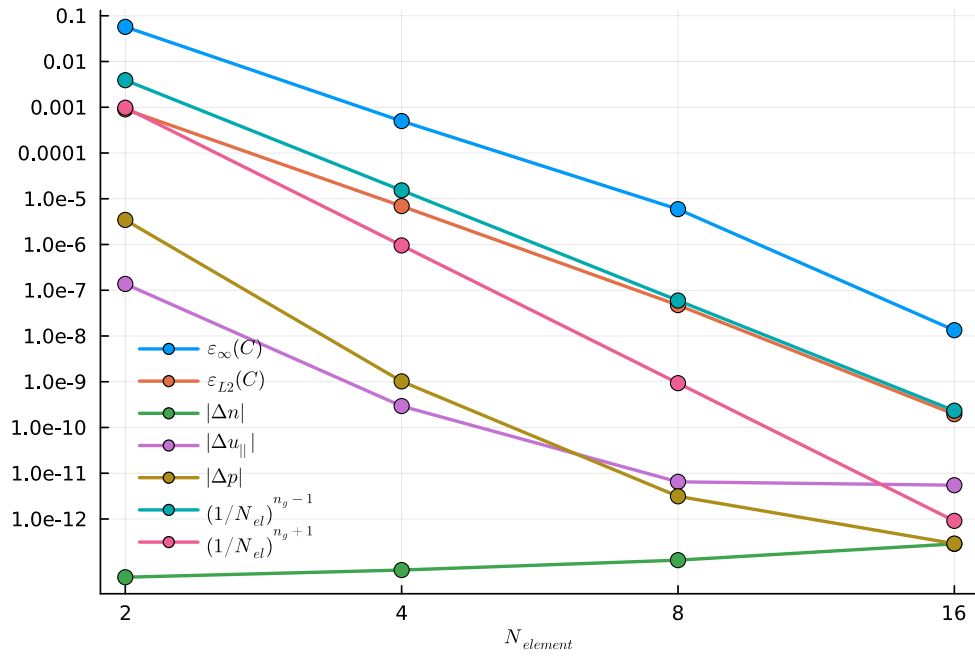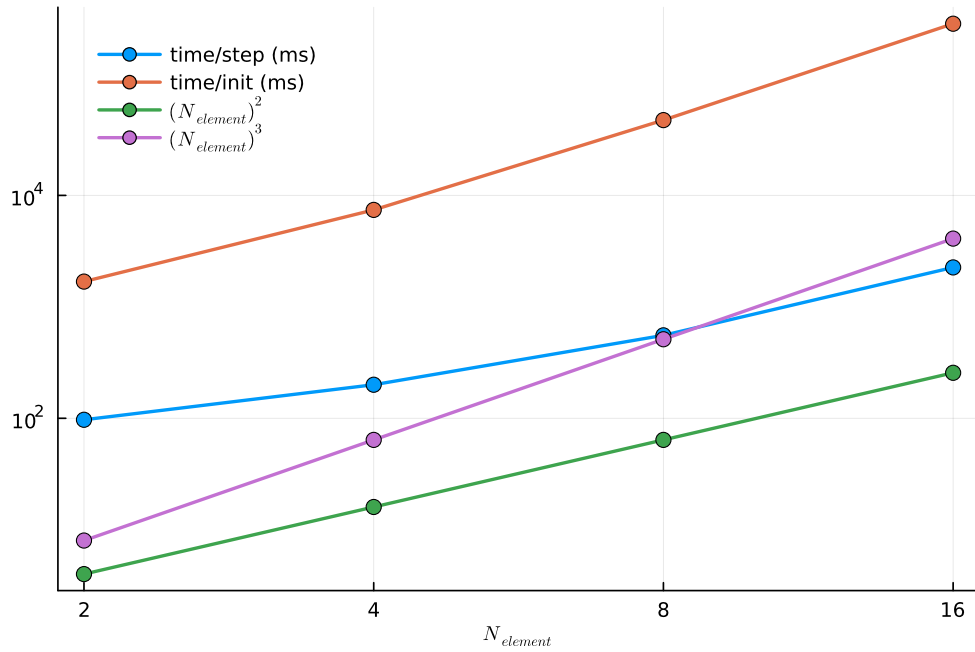
(a)

(b)

Figure 2: The numerical error and timing data for the test carried out on 2 cores with $N_{grid} = n_g = 5$ points per element.

(a)

(b)

Figure 3: The numerical error and timing data for the test carried out on 2 cores with $N_{grid} = n_g = 7$ points per element.
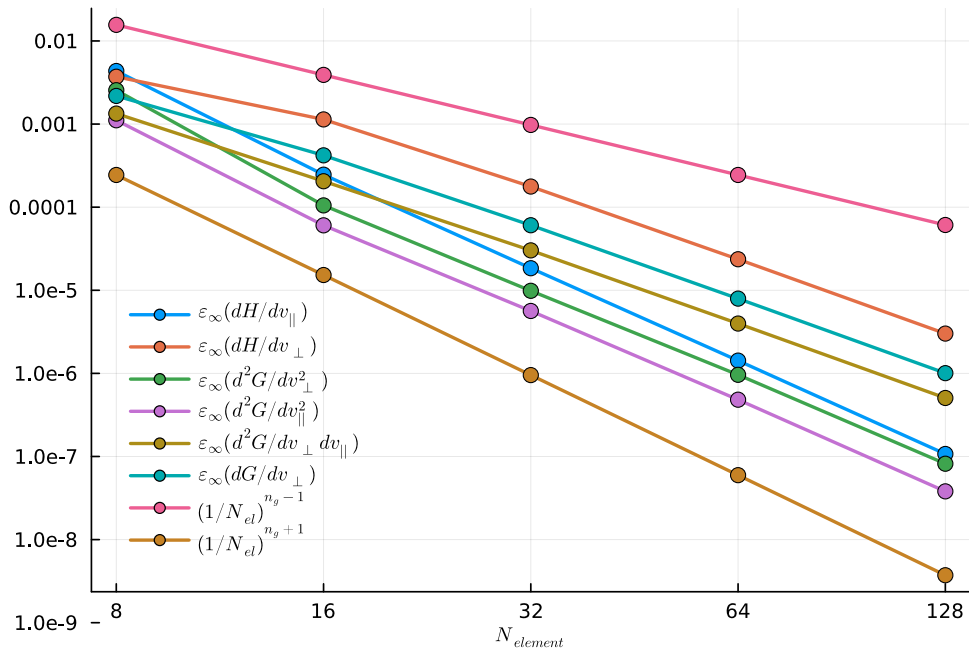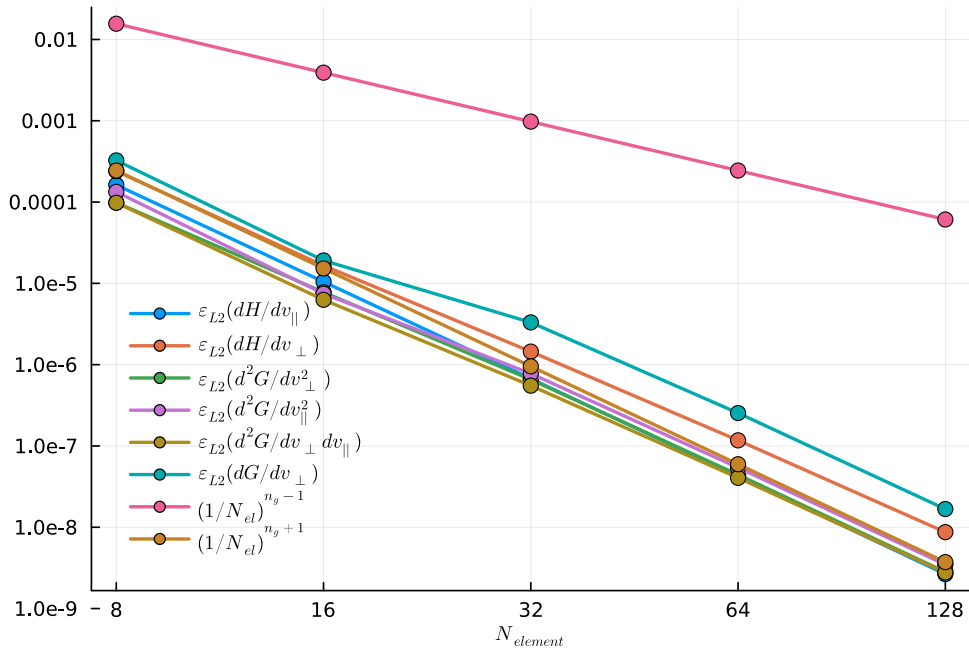
(a)

(b)

Figure 4: The numerical error and timing data for the test carried out on 2 cores with $N_{grid} = n_g = 9$ points per element.
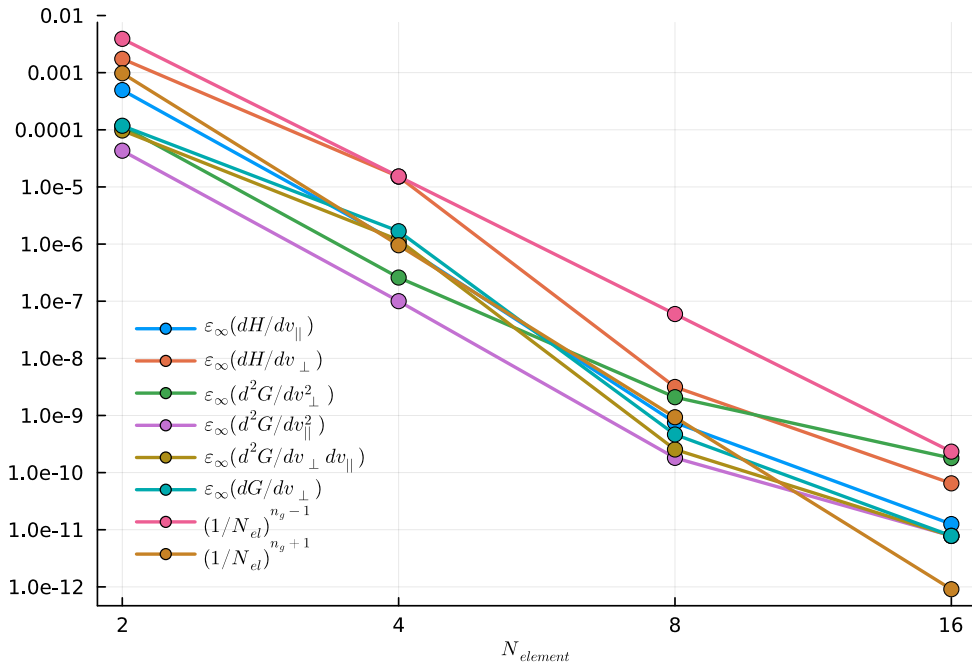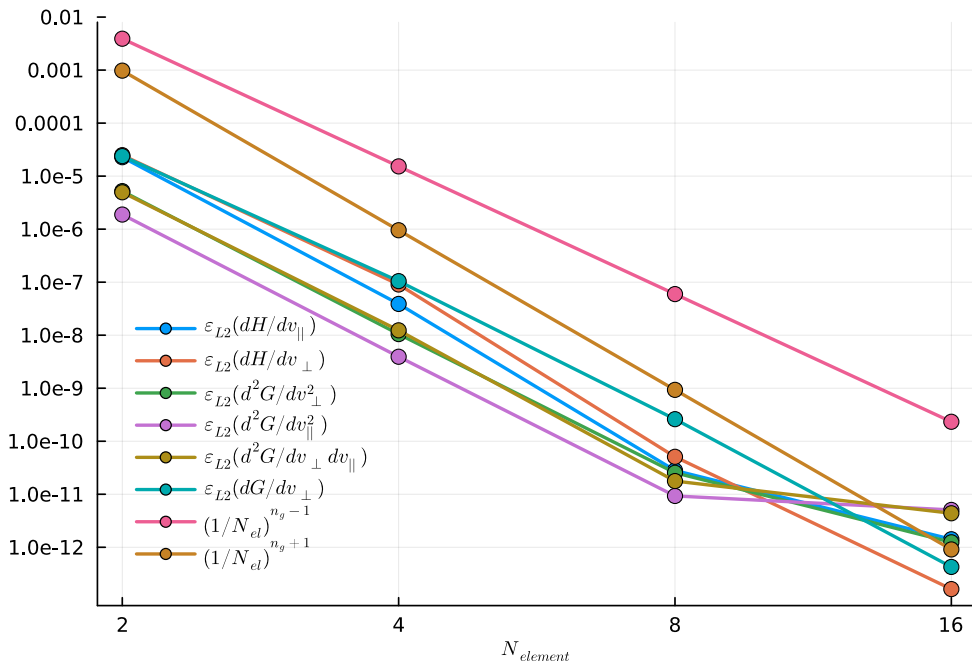
(a)

(b)

Figure 5: In figure (a) we plot the infinity norm of the error ϵ_∞ in computing the Rosenbluth potential coefficients, for $N_{grid} = 3$. In figure (b) we plot the L_2 norm of the error ϵ_{L_2} for $N_{grid} = 3$.

(a)

(b)

Figure 6: In figure (a) we plot the infinity norm of the error ϵ_∞ in computing the Rosenbluth potential coefficients, for $N_{grid} = 9$. In figure (b) we plot the L_2 norm of the error ϵ_{L_2} for $N_{grid} = 9$
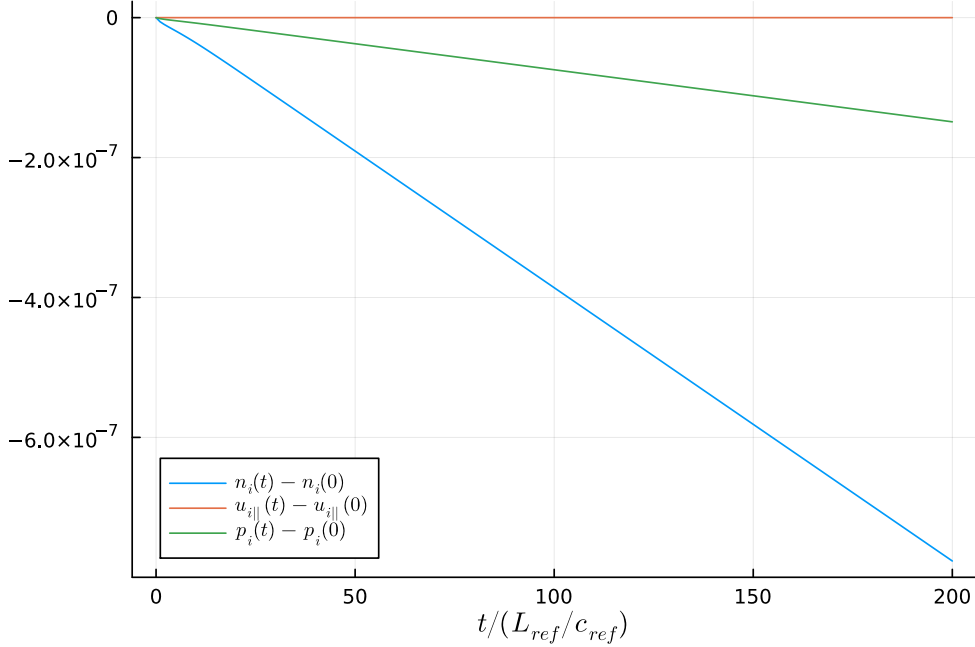
Figure 7: The changes in the first three moments of the distribution function n_s, $u_{\parallel,s}$, and p_s as a result of time evolution with the Fokker-Planck collision operator defined by equations (71) and (103) (i.e., with the numerical conserving terms). The moments are well conserved, despite the low resolution used: here we use $N_{grid} = 5$, $N_{element} = 4$ elements in the $v_\perp$ dimension and $2N_{element} = 8$ elements in the $v_\parallel$ dimension. We take the maximum velocity to be $L_\parallel = L_\perp = 6.0$. We take $\Delta t = 10^{-3}$.

distribution function

$$\ln F = \sum_{rp} \sum_{ij} \ln \left(|F_{jk}^{rp}| + \epsilon \right) \Phi_{jk}^{(rp)}, \tag{113}$$

where $\epsilon = 10^{-15}$. The approximation (113) is adequate if the solution is converging with increasing resolution in a strong sense. In figure 9 we show the L_2 norm of $F_s - F_s^M$. The simulation uses a collision frequency $\nu_{ss} = \gamma_{ss} n_{\text{ref}}/m_s^2 c_{\text{ref}}^3 = c_{\text{ref}}/L_{\text{ref}}$, and is run for a time of $200 L_{\text{ref}}/c_{\text{ref}}$. We use $N_{grid} = 5$, $N_{element} = 4$ elements in the $v_\perp$ domain, $2N_{element} = 8$ elements in the $v_\parallel$ domain, and we take the maximum velocity to be $L_\parallel = L_\perp = 3.0$. We take $\Delta t = 10^{-3}$ and we use the RK4 explicit time integration method. Despite the low resolution, the numerical solution is stable. The small errors in the moments are of order 10^{-7} at $t = 200 L_{\text{ref}}/c_{\text{ref}}$, which is larger than machine precision. To reach this time, $200 \times 1000 \times 4 \simeq 10^8$ evaluations of $C_{ss}[F_s, F_s]$ have been carried out. This might explain the errors in the moments if the correction terms have a machine-precision $\simeq 10^{-15}$ systematic bias. Simulations with increasing numerical resolution show a steady states with smaller $L_2(F_s - F_s^M)$.
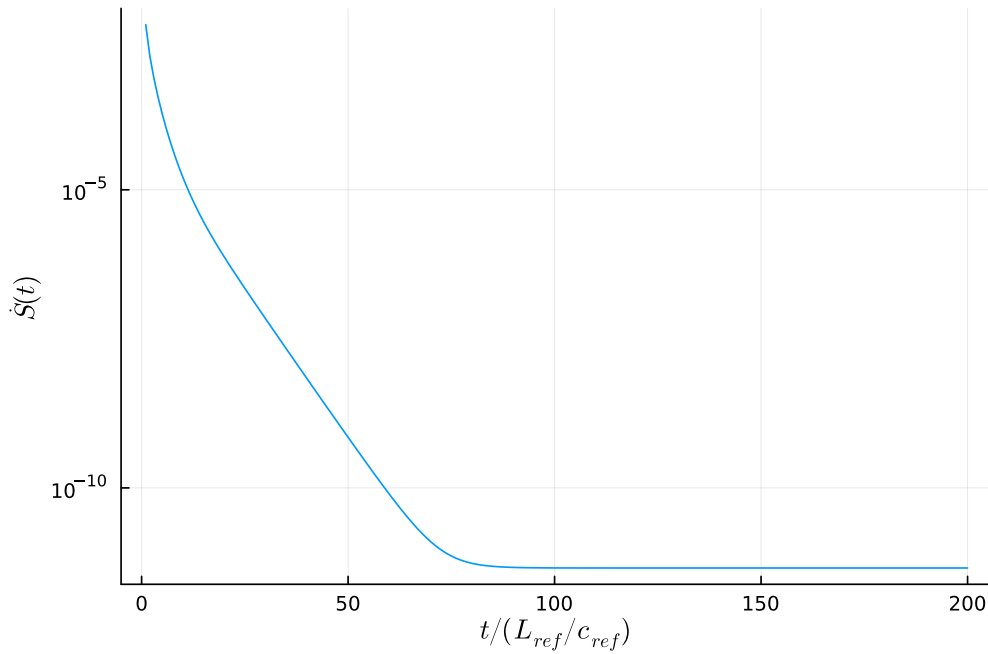
Figure 8: We plot the the entropy production $\dot{S}$, defined in equation (8). Note that $\dot{S}$ remains positive and tends to 0^+. The resolutions are provided in the main text.
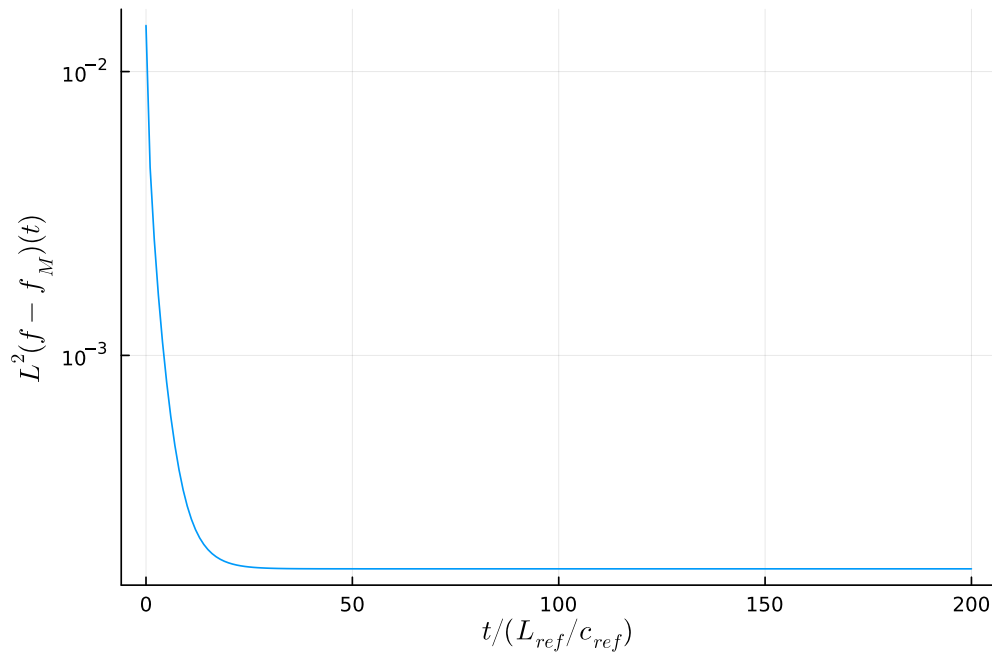

Figure 9: We plot the L_2 norm of $F_s - F_s^M$. This figure indicates that F_s becomes increasingly close to F_s^M before converging on a steady-state numerical Maxwellian. The resolutions are provided in the main text.

7. Discussion and outlook

In this report we have investigated a particular weak-form representation of the explicit Landau Fokker-Planck collision operator. We choose to use the RMJ form of the Fokker-Planck operator to permit the use of sparse elliptic solves for determining the coefficients of the nonlinear operator. We have demonstrated that this choice can lead to an optimal scaling of the cost of evaluating the operator for a single time step $\propto N_{element}^2$ with the number of elements $N_{element}$ in each of the velocity space dimensions $v_\parallel$ and $v_\perp$. We also demonstrated a successful time-evolving simulation with low resolution, demonstrating that the self-collision operator can successfully relax the distribution function to a stable steady state that is close to a Maxwellian distribution.

Unfortunately, the order unity factor in front of the expected cost scaling is large for all N_{grid}. To permit the collision operator to be routinely used in the time evolving "moment kinetics" code alongside other physics features we would ideally want to further optimise the implementation for speed. This might be achieved with an improvement to the shared-memory paralellism, distributed-memory parallelisation across nodes or through optimisations of the numerical method for speed at the cost of accuracy.

The use of distributed memory to parallelise the collision operator calculation should be fairly straightforward. The dominant costs which contribute to the time taken to evaluate the operator are the calculation of the boundary data and the assembly of the right-hand side of equation (71). Both of these steps are embarrassingly parallel.

Possible optimisations of the numerical method could involve the following. First, choosing to determine the boundary data for the elliptic solves using a multipole expansion of the Green's functions definition of G and H, equations (16) and (17), respectively. This method may permit the evaluation of the boundary data using only an order unity number of velocity integrals, providing the maximum value of $v_\parallel$ and $v_\perp$ on the grid, $L_\parallel$ and $L_\perp$, respectively, are sufficiently large. Second, choosing to evaluate the boundary data at fewer locations and constructing a larger-scale interpolation of the coefficients on the boundary might save computation time without sacrificing significant accuracy, again if $L_\parallel$ and $L_\perp$ are large enough for the Rosenbluth potential coefficients to have a simple functional form. Finally, one could choose to use a different interpolation scheme defining the right-hand side of equation (71). One could consider using the commonly used spectral-element method "quadrature crime" of assuming that mass matrices are diagonal [23] to reduce the number of operations due to the nonlinear stiffness matrices defined by equations (72) and (73).

Appendix A. Evaluating the gyroaveraged functions

To see how to evaluate the required gyroaveraged functions I_{G1}, I_{H0}, I_{H1}, and I_{H2}, consider

$$I_{G0} = \frac{1}{2\pi} \int_{-\pi}^{\pi} g \, d\vartheta', \tag{A.1}$$

as well as

$$I_{G2} = \frac{1}{2\pi} \int_{-\pi}^{\pi} g \, (\mathbf{e}_\perp \cdot \mathbf{e}'_\perp)^2 \, d\vartheta', \tag{A.2}$$

and

$$I_{G3} = \frac{1}{2\pi} \int_{-\pi}^{\pi} g \, (\mathbf{e}_\perp \cdot \mathbf{e}'_\perp \times \mathbf{b})^2 \, d\vartheta'. \tag{A.3}$$

We note that $\mathbf{e}_\perp \cdot \mathbf{e}'_\perp = \cos(\vartheta' - \vartheta)$ and $\mathbf{e}_\perp \cdot \mathbf{e}'_\perp \times \mathbf{b} = \sin(\vartheta - \vartheta')$. Expanding g, we have that

$$I_{G0}(v_\parallel, v_\perp, v'_\parallel, v'_\perp) = \frac{1}{2\pi} \int_{-\pi}^{\pi} \left((v_\parallel - v'_\parallel)^2 + v_\perp^2 + v'^{\,2}_\perp - 2v_\perp v'_\perp \cos(\vartheta' - \vartheta) \right)^{1/2} d\vartheta'. \tag{A.4}$$

Here we can recognise an Elliptic integral. Suitable rearrangement and relabeling give us

$$I_{G0}(v_\parallel, v_\perp, v'_\parallel, v'_\perp) = \frac{2}{\pi} \left((v_\parallel - v'_\parallel)^2 + (v_\perp + v'_\perp)^2 \right)^{1/2} E(m(v_\parallel, v_\perp, v'_\parallel, v'_\perp)) \tag{A.5}$$

with

$$m(v_\parallel, v_\perp, v'_\parallel, v'_\perp) = 4 v_\perp v'_\perp \left((v_\parallel - v'_\parallel)^2 + (v_\perp + v'_\perp)^2 \right)^{-1} \tag{A.6}$$

and we have used the definition of the complete elliptic integral of the first kind

$$K(m) = \int_0^{\pi/2} \frac{1}{\sqrt{1 - m \sin^2 \theta}} \, d\theta \tag{A.7}$$

Complete elliptic integral of the second kind

$$E(m) = \int_0^{\pi/2} \sqrt{1 - m \sin^2 \theta} \, d\theta \tag{A.8}$$

The remaining integrals are

$$I_{G1}(v_\parallel, v_\perp, v'_\parallel, v'_\perp) = $$
$$-\frac{2}{\pi} \left((v_\parallel - v'_\parallel)^2 + (v_\perp + v'_\perp)^2 \right)^{1/2} \left(\frac{2 - m}{3m} E(m) - \frac{2}{3} \frac{(1 - m)}{m} K(m) \right) \tag{A.9}$$

$$I_{G2}(v_\parallel, v_\perp, v'_\parallel, v'_\perp) = $$
$$\frac{2}{\pi} \left((v_\parallel - v'_\parallel)^2 + (v_\perp + v'_\perp)^2 \right)^{1/2} \frac{1}{15m^2} \left((7m^2 + 8m - 8)E(m) + 4(2 - m)(1 - m)K(m) \right) \tag{A.10}$$

$$I_{G3}(v_\parallel, v_\perp, v'_\parallel, v'_\perp) = $$
$$\frac{2}{\pi} \left((v_\parallel - v'_\parallel)^2 + (v_\perp + v'_\perp)^2 \right)^{1/2} \frac{1}{15m^2} \left(8(m^2 - m + 1)E(m) - 4(2 - m)(1 - m)K(m) \right) \tag{A.11}$$

where we have used the identities

$$\int_0^{\pi/2} \sin^2\theta \sqrt{1 - m\sin^2\theta}\, d\theta = \frac{1-m}{3m}K(m) + \frac{2m-1}{3m}E(m) \tag{A.12}$$

$$\int_0^{\pi/2} \sin^4\theta \sqrt{1 - m\sin^2\theta}\, d\theta = \frac{1}{15m^2}\left(2(2m+1)(1-m)K(m) + (8m^2 - 3m - 2)E(m)\right) \tag{A.13}$$

$$\int_0^{\pi/2} (1 - 2\sin^2\theta)\sqrt{1 - m\sin^2\theta}\, d\theta = \frac{2-m}{3m}E(m) - \frac{2}{3}\frac{(1-m)}{m}K(m) \tag{A.14}$$

$$\int_0^{\pi/2} (1 - 2\sin^2\theta)^2 \sqrt{1 - m\sin^2\theta}\, d\theta = \frac{1}{15m^2}\left((7m^2 + 8m - 8)E(m) + 4(2-m)(1-m)K(m)\right) \tag{A.15}$$

$$\int_0^{\pi/2} \left(1 - (1 - 2\sin^2\theta)^2\right)\sqrt{1 - m\sin^2\theta}\, d\theta$$

$$= \frac{1}{15m^2}\left(8(m^2 - m + 1)E(m) - 4(2-m)(1-m)K(m)\right) \tag{A.16}$$

If we wish to evaluate directly the integral equations for $\partial H_{s'}/\partial v_\parallel$ and $\partial H_{s'}/\partial v_\perp$ then we require the following elliptic integrals

$$I_{H0} = \frac{1}{2\pi}\int_{-\pi}^{\pi} \frac{1}{g}\, d\vartheta', \tag{A.17}$$

$$I_{H1} = \frac{1}{2\pi}\int_{-\pi}^{\pi} \frac{\mathbf{e}_\perp \cdot \mathbf{e}_\perp'}{g}\, d\vartheta', \tag{A.18}$$

and

$$I_{H2} = \frac{1}{2\pi}\int_{-\pi}^{\pi} \frac{(\mathbf{e}_\perp \cdot \mathbf{e}_\perp')^2}{g}\, d\vartheta'. \tag{A.19}$$

Using the methods described above, we find that

$$I_{H0} = \frac{2}{\pi}\left((v_\parallel - v_\parallel')^2 + (v_\perp + v_\perp')^2\right)^{-1/2} K(m), \tag{A.20}$$

$$I_{H1} = -\frac{2}{\pi}\left((v_\parallel - v_\parallel')^2 + (v_\perp + v_\perp')^2\right)^{-1/2}\left(\frac{m-2}{m}K(m) + \frac{2}{m}E(m)\right), \tag{A.21}$$

and

$$I_{H2} = \frac{2}{\pi}\left((v_\parallel - v_\parallel')^2 + (v_\perp + v_\perp')^2\right)^{-1/2}\left(\frac{3m^2 - 8m + 8}{3m^2}K(m) + \frac{4m-8}{3m^2}E(m)\right). \tag{A.22}$$

Here we have used that

$$\int_0^{\pi/2} \left(1 - 2\sin^2\theta\right)\left(1 - m\sin^2\theta\right)^{-1/2} d\theta = \frac{m-2}{m}K(m) + \frac{2}{m}E(m), \tag{A.23}$$

and

$$\int_0^{\pi/2} \left(1 - 2\sin^2\theta\right)^2 \left(1 - m\sin^2\theta\right)^{-1/2} d\theta = \frac{3m^2 - 8m + 8}{3m^2}K(m) + \frac{4m-8}{3m^2}E(m). \tag{A.24}$$
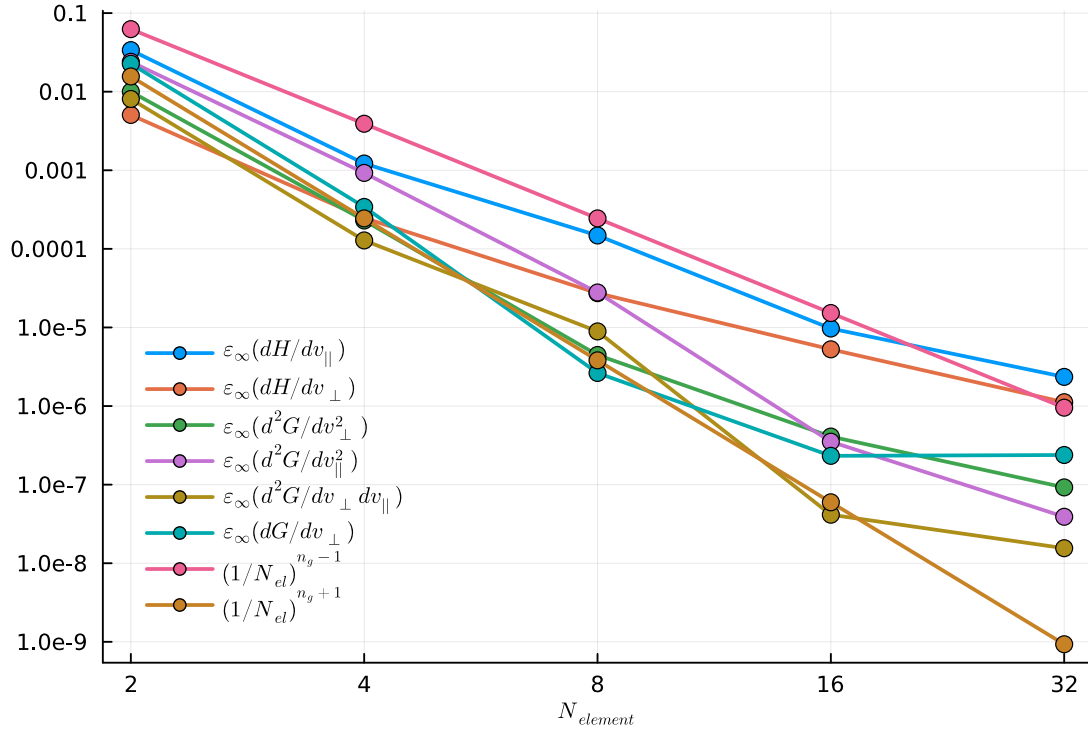
Figure B1: We plot the infinity norm of the errors ϵ of the potentials $\partial H/\partial v_\parallel$, $\partial H/\partial v_\perp$, $\partial G/\partial v_\perp$, $\partial^2 G/\partial v_\perp^2$, $\partial^2 G/\partial v_\parallel^2$, $\partial^2 G/\partial v_\perp \partial v_\parallel$ for a Maxwellian input distribution, compared to the expected scalings for differentiation and integration, equations (111) and (112), respectively.

Appendix B. Computing the Rosenbluth potentials by direct integration

A more direct, but less efficient, method for computing the Rosenbluth potentials is to use the integral expressions (47)-(52) for all $(v_\parallel, v_\perp)$ rather than just the boundary values. Here we show the results of such a calculation to demonstrate the correct implementation of (47)-(52) and the results in Appendix A.

In figure B1 we plot the infinity-norm errors on the calculation by direct integration of the derivatives of the Rosebluth potentials for a Maxwellian input, for which the results are known analytically (see e.g. [22]). We see that the integration error becomes small for increasing resolution, indicating that the definitions of the integrands are correct. However, the errors eventually deviate from the expected scaling. This is due to problems carrying out the integral accurately in the region on the integrand where $\mathbf{v}'$ is such that $F_s(\mathbf{v}') \sim \mathrm{O}\,(1)$. This problem might be addressed with an improved integration quadrature, or by using higher than double precision to compute the integrand. Note that this difficulty does not affect the integration of the potentials in the far-field region at the velocity space boundary – meaning that machine-precision accuracy can be achieved in the numerical method presented in the main text. This is evident from figures 5 and 6. The script used to generate figure B1 may be found at

the following URL: `https://github.com/mabarnes/moment_kinetics/blob/merge_fkpl_collisions/test_scripts/fkpl_direct_integration_test.jl`.

[1] Kardar M 2007 *Statistical Physics of Particles* (Cambridge University Press)

[2] Dellar P *Kinetic Theory* University of Oxford Master Course in Mathematical and Theoretical Physics: lecture series. URL `https://people.maths.ox.ac.uk/dellar/MMPkinetic.html`

[3] Rosenbluth M N, MacDonald W M and Judd D L 1957 *Phys. Rev.* **107** 1–6

[4] Hazeltine R D and Meiss J D 2003 *Plasma Confinement* (New York: Dover)

[5] Helander P and Sigmar D J 2002 *Collisional Transport in Magnetized Plasmas* (Cambridge, UK: Cambrige University Press)

[6] Parra F I *Collisional Plasma Physics: (I) Fokker-Planck collision operator* University of Oxford Master Course in Mathematical and Theoretical Physics: 2019 lecture series. URL `https://www-thphys.physics.ox.ac.uk/people/FelixParra/CollisionalPlasmaPhysics/CollisionalPlasmaPhysics.html`

[7] Alouani-Bibi F, Shoucri M and Matte J P 2004 *Computer physics communications* **164** 60–66

[8] Pataki A and Greengard L 2011 *Journal of Computational Physics* **230** 7840–7852

[9] Hirvijoki E and Adams M F 2017 *Phys. Plasmas* **24** 032121

[10] Abazorius M 2023 *University of Oxford* DPhil Thesis *(In Progress)*

[11] Wilkie G J, Keßler T and Rjasanow S 2023 *Comput. Phys. Commun.* **291** 108812

[12] Catto P J and Simakov A N 2004 *Phys. Plasmas* **11** 90

[13] Hinton F L and Hazeltine R D 1976 *Rev. Mod. Phys.* **48** 239–308

[14] Catto P J and Tsang K T 1977 *Phys. Fluids* **20** 396–401

[15] Abel I G, Barnes M, Cowley S C, Dorland W and Schekochihin A A 2008 *Phys. Plasmas* **15** 122509

[16] Barnes M, Abel I, Dorland W, Ernst D, Hammett G, Ricci P, Rogers B, Schekochihin A and Tatsuno T 2009 *Phys. Plasmas* **16**

[17] Sugama H, Watanabe T H and Nunami M 2009 *Phys. Plasmas* **16** 112503

[18] Abel I G, Plunk G G, Wang E, Barnes M, Cowley S C, Dorland W and Schekochihin A A *Rep. Prog. Phys.* **76** 116201

[19] Parra F I *Collisionless Plasma Physics: (II) Drift-Kinetics* University of Oxford Master Course in Mathematical and Theoretical Physics: 2019 lecture series. URL `https://www-thphys.physics.ox.ac.uk/people/FelixParra/CollisionlessPlasmaPhysics/CollisionlessPlasmaPhysics.html`

[20] Boyd J P 2001 *Chebyshev and Fourier Spectral Methods* (Dover)

[21] Barnes M, Parra F I, Hardman M R and Omotani J 2021 *Excalibur/Neptune Report* 2047357–TN–D2.2+M2.5

[22] Hardman M R, Omotani J, Barnes M, Newton S L and Parra F I 2023 *Excalibur/Neptune Report* 2070839–TN–06

[23] Teukolsky S A 2015 *J. Comput. Phys.* **283** 408–413